NASA CONTRACTOR REPORT

NASA CR-2818

GRADIENTS OF METEOROLOGICAL PARAMETERS IN CONVECTIVE AND NONCONVECTIVE AREAS

Milton S. McCown and James R. Scoggins

Prepared by
TEXAS A&M UNIVERSITY
College Station, Tex. 77843
for George C. Marshall Space Flight Center

NATIONAL AERONAUTICS AND SPACE ADMINISTRATION • WASHINGTON, D. C. • MARCH 1977

1 REPORT NO.	2. GOVERNMENT ACCESSION NO.	3. RECIPIENT'S CATALOG NO.
NASA CR-2818		

4 TITLE AND SUBTITLE	5. REPORT DATE
Gradients of Meteorological Parameters in Convective and Nonconvective Areas	March 1977
	6. PERFORMING ORGANIZATION CODE

7. AUTHOR(S)	8. PERFORMING ORGANIZATION REPORT #
Milton S. McCown and James R. Scoggins	M-214

9. PERFORMING ORGANIZATION NAME AND ADDRESS	10. WORK UNIT NO.
Center for Applied Geosciences College of Geosciences Texas A&M University College Station, Texas 77843	11. CONTRACT OR GRANT NO. NAS8-31773

12 SPONSORING AGENCY NAME AND ADDRESS	13. TYPE OF REPORT & PERIOD COVERED
National Aeronautics and Space Administration Washington, D. C. 20546	Contractor
	14. SPONSORING AGENCY CODE

15. SUPPLEMENTARY NOTES

16. ABSTRACT

Horizontal gradients of geopotential height, temperature, and wind speed were computed at the 850-, 700-, 500-, and 200-mb levels by using data from the National Aeronautics and Space Administration's second and fourth Atmospheric Variability Experiments (AVE). Mixing ratio gradients also were computed, but only for the 850-, 700-, and 500-mb levels. These AVE experiments, conducted on 11-12 May 1974 and 24-25 April 1975, respectively, provided rawinsonde data at 3- to 6-h intervals. Cumulative frequency distributions and statistical parameters showed that the variability and magnitude of the gradients decreased as the gradients were computed over progressively longer distances. Most frequency distributions were positively skewed, and the standard deviations of the gradient distributions were roughly half as large as the means.

An examination of the differences of gradients observed in convective and nonconvective areas was made after convective areas were determined objectively using Manually Digitized Radar data. In both experiments the gradients of height, wind speed, and mixing ratio at 850 mb were larger in convective than nonconvective areas. No general relationship held for the meteorological variables at other levels.

Intensive examination of the gradients observed near squall lines revealed typical gradient patterns and trends in the magnitudes of the gradients associated with convective systems. Height gradients at 850 mb were largest ahead of the storms, but the gradients of other meteorological variables and height gradients at other levels were largest in the storm areas or following the storms. Such patterns were maintained throughout much of the life cycle of the storms.

17. KEY WORDS	18. DISTRIBUTION STATEMENT
	47

19. SECURITY CLASSIF. (of this report)	20. SECURITY CLASSIF. (of this page)	21. NO. OF PAGES	22. PRICE
Unclassified	Unclassified	93	$5.50

FOREWORD

This report is one of several to be published from research conducted under NASA Contract NAS8-31773 entitled, "Relationships Between Severe Storms and Their Environment." This effort is sponsored by the NASA Office of Applications under the direction of Marshall Space Flight Center's Aerospace Environment Division. The results presented in this report represent only a portion of the total research effort. Data used in the report were taken from the AVE II and AVE IV Experiments.

AUTHORS' ACKNOWLEDGEMENTS

The authors thank Dr. Aylmer H. Thompson, Dr. Glen N. Williams, and Dr. Kenneth C. Brundidge for reviewing the final manuscript and Mr. Kelly Hill of NASA for his encouragement and advice. Gratitude and appreciation are extended to Katy Capt and Libby Pearson for typing and to Ginny Smith for work on graphs and figures.

The authors gratefully acknowledge support provided under NASA Contract No. NAS8-31773. This contract is under the auspices of the Aerospace Environment Division, Space Sciences Laboratory, National Aeronautics and Space Administration, Marshall Space Flight Center, Alabama.

TABLE OF CONTENTS

TABLE OF CONTENTS (Continued)

LIST OF TABLES

LIST OF FIGURES

LIST OF FIGURES (Continued)

GRADIENTS OF METEOROLOGICAL PARAMETERS IN CONVECTIVE AND NONCONVECTIVE AREAS

by Milton S. McCown[1] and James R. Scoggins[2]

Center for Applied Geosciences, Texas A&M University

1. INTRODUCTION

a. Statement of problem

From basic meteorological theory, it is known that the relationships between many variables involve horizontal gradients. For example, the equations of motion relate wind speed to pressure gradient, and the thermal wind equation relates vertical wind shear to the horizontal temperature gradient. The study of gradients may help in an understanding of the processes leading to convection and to its subsequent development and dissipation. Furthermore, the study of gradients of meteorological variables should help determine to what extent convection alters the synoptic environment of storm areas.

Basic research into the interrelationships between meso- and synoptic-scale systems has been in progress for several years, but there is still insufficient knowledge of such interactions. Yet, it is known that mesoscale systems produce much convective-type precipitation, and that significant interactions between convective- and synoptic-scale systems occur (Ninomiya, 1971a). The study of the gradients involved should increase the understanding of such interactions.

A basic problem in the study of the dynamic or kinematic aspects of any mesoscale system is that of resolution. Since such studies require better temporal or spatial resolutions than that provided by the operational rawinsonde network, supplementary data must be collected by the use of satellites, aircraft, or special rawinsonde systems. The Atmospheric Variability Experiments (AVE) conducted by the National Aeronautics and Space Administration (NASA) furnished data taken at 3- or 6-h intervals instead of the usual 12-h intervals; thus, the AVE experiments provided rawinsonde data of a better temporal resolution that that measured operationally, though the spatial resolution remained the same.

---

[1] Graduate Assistant

[2] Professor of Meteorology

In this research, the magnitudes of the gradients of several meteorological variables are determined for convective and nonconvective areas using data collected from 1200 GMT on 11 May through 1200 GMT on 12 May 1974 for AVE II, and from 0000 GMT on 24 April through 1200 GMT on 25 April 1975 for AVE IV.

b. Objectives

The principal objective of this research is to determine the distribution of gradients in convective and nonconvective areas and how the gradients differ between these areas.

Specific objectives include the following:

(1) Determine cumulative frequency distributions of the magnitudes of horizontal gradients of temperature, geopotential height, wind speed, and mixing ratio at several pressure levels in the atmosphere.

(2) Examine the differences between statistical parameters of the gradients of each of the four meteorological variables over convective and nonconvective areas.

(3) Examine the interaction between the storm areas and the synoptic field by a comparison of the means of gradients in the convective and nearby nonconvective areas at successive time intervals during the life cycle of a convective system.

c. Previous studies

Most previous studies involving horizontal atmospheric gradients have been on a mesoscale basis. These studies have tended to concentrate on short-lived phenomena such as clear air turbulence (CAT) or convective activity. In order to study mesoscale systems, several different approaches have been used that involve statistical or observational techniques. Many of the studies involving gradients have concentrated on the gradients of a single variable.

Most information involving either gradients of wind speed or vector shear have come from the mesoscale study of clear air

turbulence. By using airplane data from over the western United States, Scoggins (1975) has shown that CAT at 300 mb occurred 71% of the time when the magnitude of the vector horizontal wind shear exceeded 4.5×10^{-5} sec^{-1}. The horizontal grid spacing used in the calculations was approximately 158 km. Boucher (1973) noted a wind speed gradient of 1.23×10^{-4} sec^{-1} in an area of moderate clear air turbulence at 500 mb near Wallops Island, Virginia, on 4 February 1970. His data came from a network of eight special rawinsonde stations 100 km apart.

Results from mesoscale studies of other variables reveal that horizontal temperature gradients often fail to support the vertical shear that is present in an occlusion nor in the vicinity of jet streams (Kreitzberg, 1968), or in squall lines (Fankhauser, 1969). It also was determined that direct analysis of geopotential height gradients on a mesoscale basis would not give reliable results because of the random errors in accuracy and limitations of surface pressure data used in the individual soundings. Consistent results were obtained for the height field, however, by deriving the horizontal height perturbations associated with mesoscale winds. Such an analysis revealed that the largest height gradients across a squall line occurred at 575 mb (Fankhauser, 1974).

Numerous studies have led to the conclusion that mesoscale systems embedded within the general synoptic-scale weather pattern are often responsible for the development and maintenance of convective activity (Fankhauser, 1969; Lewis et al., 1974). An investigation of horizontal gradients which can be related to convective processes has been an essential part of some of these studies.

A major problem in the study of atmospheric gradients has been that of adequate spatial and/or temporal resolution. House (1960) concluded that the average upper-air network spacing of 220 n mi with intervals of 12 h between rawinsonde releases was insufficient for the study of gradients occurring during the life cycle of an instability line. However, it has been determined that a closer

network of stations with more frequent time intervals, such as that provided by the National Severe Storms Laboratory in Oklahoma, can provide a consistent data base of meteorological variables, though gradients relevant to individual thunderstorm circulations were either not detected at all, or were filtered in the data-handling process (Fankhauser, 1969).

In one study of mesoscale systems, statistical methods were used to establish relationships between clouds or radar echoes and various combinations of temperature and geopotential height gradients (Scoggins et al., 1972). Four periods of three days each, scattered throughout the year, were used in the study, and it was determined that during three of the four periods, correlation coefficients statistically significant at the 5% level existed between the 850- and 500-mb geopotential height gradients when echoes were observed by radar within 100 n mi of the rawinsonde stations. When echoes were not observed, a significant correlation coefficient existed during two of the four periods. There was very little consistency between the periods, however, and thus no systematic trend between the periods was established.

The use of gradients of selected atmospheric variables as predictors of convective activity has been advocated by some investigators. Reap and Alaka (1969) have reported that the 1000-mb dew point gradient was one of the better indices out of 43 tested in indicating severe storm activity 24 h in advance. In their study, a Lagrangian model used three-dimensional air parcel trajectories to generate prognostic fields of temperature and moisture. The severe storm activity occurred along the line of maximum dew point gradients to the west of the moisture axis. The existence of destabilization centers in the strong thermal gradient on the west side of the thermal ridge has been shown by Harley (1971). Such centers result from differential advection of the stability field. Miller (1969) also has reported the existence of steep horizontal temperature and moisture gradients over and upwind from areas where there was the threat of severe

convective activity. Warmer and drier air to the west or southwest of the threatened area was a significant synoptic feature.

In addition to the existence of significant gradients in an area preceding an outbreak of convection, there is evidence that after the storms have formed the interaction between the large-scale field and convective regions tends to intensify the gradients of moisture and temperature in the rear portion of the convective area. Ninomiya (1971a) used data from the conventional 12-h synoptic time periods combined with ATS III pictures to produce detailed synoptic and dynamic analyses. He concluded that the release of latent heat over the convective area resulted in the formation of a warm core in the middle troposphere, which increased horizontal thermal gradients to the northwest of the storm area and resulted in the formation of a strong jet stream in this region. Dynamically forced downward motion occurred in the left rear portion of the storm area because the thermal wind blew from an area of smaller to larger vorticity. The mixing ratio in the left rear portion of the storm area decreased and caused an intensification of the mixing ratio gradient occurring between the storm areas and the dry areas to their rear. A schematic model was developed to explain the interactions between the convective system and the large-scale field through the transfer of energy between synoptic- and convective-scale systems.

It has been shown in the previous studies that strong horizontal moisture and temperature gradients existed upwind from areas that were threatened by an outbreak of severe thunderstorm activity. Furthermore, the moisture and temperature gradients in the rear portion of storm areas were intensified by the interaction between the large-scale field and the convective region, and a high tropospheric jet stream was likely to be associated with these changes. These conclusions have been based upon mesoscale data from only limited areas such as the NSSL network, or from the operational 12-h rawinsonde network. Furthermore, no attempt has been made to relate objectively the strength of the convective

system to the strength of associated atmospheric gradients. In previous studies, the changes of the gradients observed over periods of less than 12 h have had to be inferred. By using the AVE data, the gradients of the meteorological variables can be calculated at 3- to 6-h intervals, and the use of Manually Digitized Radar (MDR) data will allow an objective examination of the relationship between the strength of a convective system and its associated gradients.

2. DATA

a. AVE data

The data used to produce fields of the atmospheric variables came from the AVE II experiment and from the AVE IV experiment. Both experiments utilized data from most of the rawinsonde stations in the United States east of 105° west longitude. The AVE data were collected during carefully selected time periods of 36 to 48 h when rapid changes in weather patterns occurred, and the rawinsonde ascents were made at either 3- or 6-h intervals instead of the usual 12-h intervals.

Fifty-four rawinsonde stations participated in the AVE II experiment with the soundings commencing at 1200 GMT on 11 May 74, and ending at 1200 GMT on 12 May 1974. Figure 1 shows the locations and stations identifiers* of the stations participating in AVE II.

Forty-two rawinsonde stations participated in the AVE IV experiment covering nearly the same area as that in AVE II, with the exception of areas in the extreme northern and southern regions where most of the additional rawinsonde stations in AVE II were located. Soundings were taken at nine times during AVE IV; 24 April 1975 at 0000 GMT, 0600 GMT, 1200 GMT, 1500 GMT, 1800 GMT, and 2100 GMT, and on 25 April 1975 at 0000 GMT, 0600 GMT, and 1200 GMT. The station identifiers* and locations of the stations participating in AVE IV are shown in Fig. 2.

The data reduction processes used for the data of AVE II and AVE IV were similar. Personnel from NASA's Marshall Space Flight Center, Alabama and Texas A&M University worked in conjunction on both experiments. To determine wind velocities, angle data were extracted at 30-sec intervals, and thermodynamic quantities were computed from ordinate data for each pressure contact. To insure accuracy, the input data were checked for errors by calculating centered differences, and the errors were then corrected. Computed soundings were then rechecked and corrections were made

*Station names are given in the Appendix.

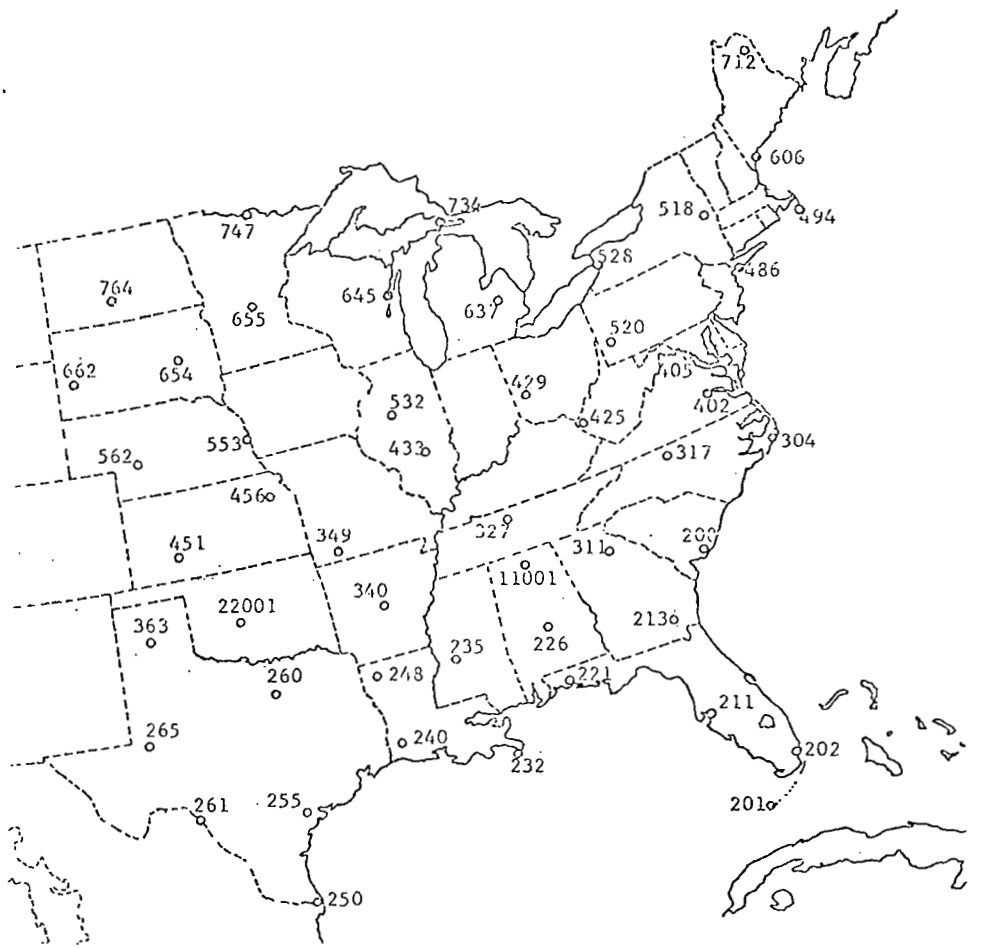

Fig. 1. Locations of rawinsonde stations for AVE II.

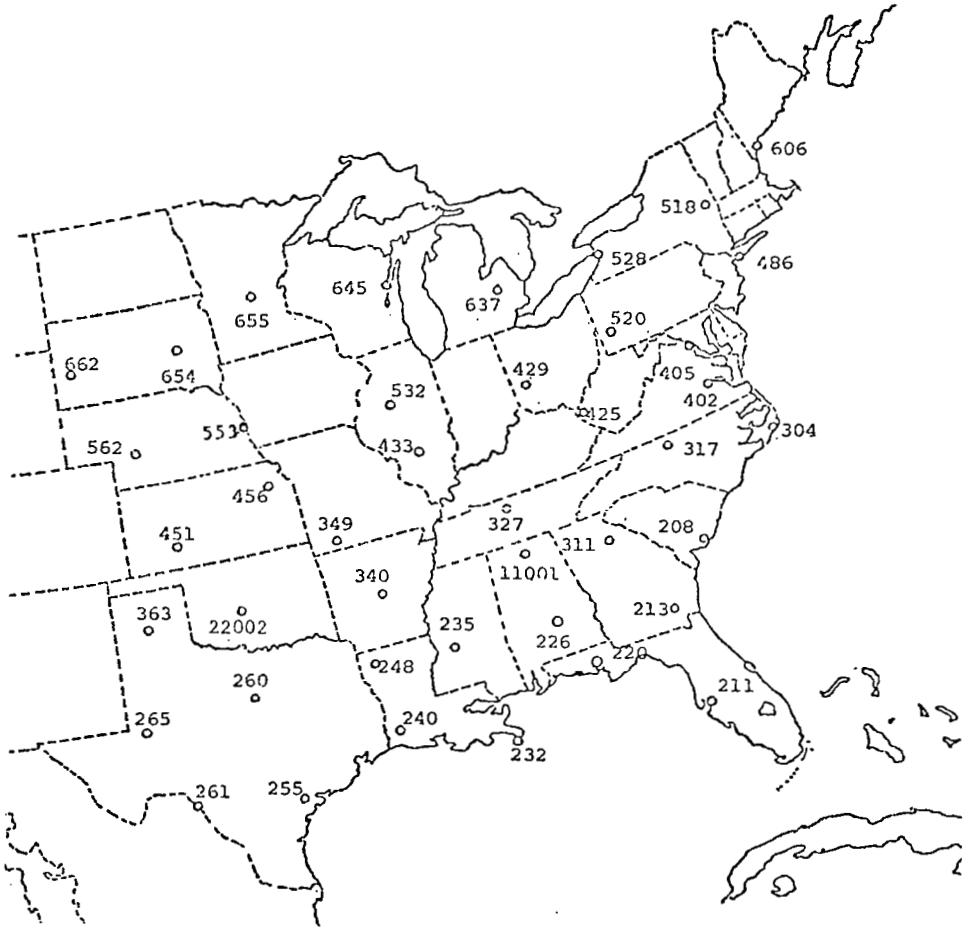

Fig. 2. Locations of rawinsonde stations for AVE IV.

(Scoggins and Turner, 1975; Fucik and Turner, 1975). The data reduction procedure for AVE IV was changed slightly from that used in AVE II. These changes involved humidity and wind velocity computations and are described in more detail by Fuelberg (Fuelberg and Turner, 1975). The 25-mb interval data for AVE II are given by Scoggins and Turner (1975), and for AVE IV by Fucik and Turner (1975).

Estimates of the RMS errors in the thermodynamic quantities for both AVE II and AVE IV are as follows (Scoggins and Smith, 1973; Fuelberg, 1974).

Parameter	Approximate RMS Error
Temperature	1°C
Pressure	1.3 mb surface to 400 mb
	1.1 mb between 400 and 100 mb
Humidity	10%
Pressure Altitude	10 gpm at 500 mb
	20 gpm at 300 mb
	50 gpm at 50 mb

Maximum RMS vector errors in wind speed for the AVE II and AVE IV data are based on the worst geometric tracking configurations possible. Fuelberg (1974) indicates these errors as follows.

Level	Elevation Angle	
	40°	10°
700 mb	0.5 m s^{-1}	2.5 m s^{-1}
500 mb	0.8 m s^{-1}	4.5 m s^{-1}
300 mb	1.0 m s^{-1}	7.8 m s^{-1}

The computer program for data reduction and error analysis for AVE II, with only slight modifications for AVE IV, is given by Fuelberg (1974).

b. Manually Digitized Radar data

Manually Digitized Radar (MDR) data obtained from the National Oceanic and Atmospheric Administration's (NOAA) Techniques Development Laboratory were used to determine the coverage and intensity of precipitation for both AVE II and AVE IV. The MDR grid network, composed of grid blocks approximately 83 km on a side, covers most of the United States, and is shown in Fig. 3.

The MDR code assigns to each radar box a code number ranging from 0 to 9 depending upon the maximum observed echo intensity and areal extent of precipitation within that box. Reap (1975) has indicated thunderstorm activity by an MDR code number of 4 or greater, and rainshower activity by MDR values of 2 or 3. Additional information about the MDR code is given below (Foster and Reap, 1973).

Code No.	Maximum Observed VIP[1] Values	Coverage in Box	Maximum Rainfall Rate (in./hr)	Intensity Category
0	No Echoes			
1	1	any VIP1	<.1	Weak
2	2	≤ 50% of VIP2	.1- .5	Moderate
3	2	> 50% of VIP2	.5-1.0	Moderate
4	3	≤ 50% of VIP3	1.0-2.0	Strong
5	3	> 50% of VIP3	1.0-2.0	Strong
6	4	≤ 50% of VIP3 and 4	1.0-2.0	Very Strong
7	4	> 50% of VIP3 and 4	1.0-2.0	Very Strong
8	5 or 6	≤ 50% of VIP3 4, 5, and 6	>2.0	Intense or Extreme
9	5 or 6	> 50% of VIP3, 4, 5, and 6	>2.0	Intense or Extreme

[1]Video Integrator Processor

Hourly MDR reports were plotted for the time periods of the AVE II and AVE IV experiments and composite charts determined by

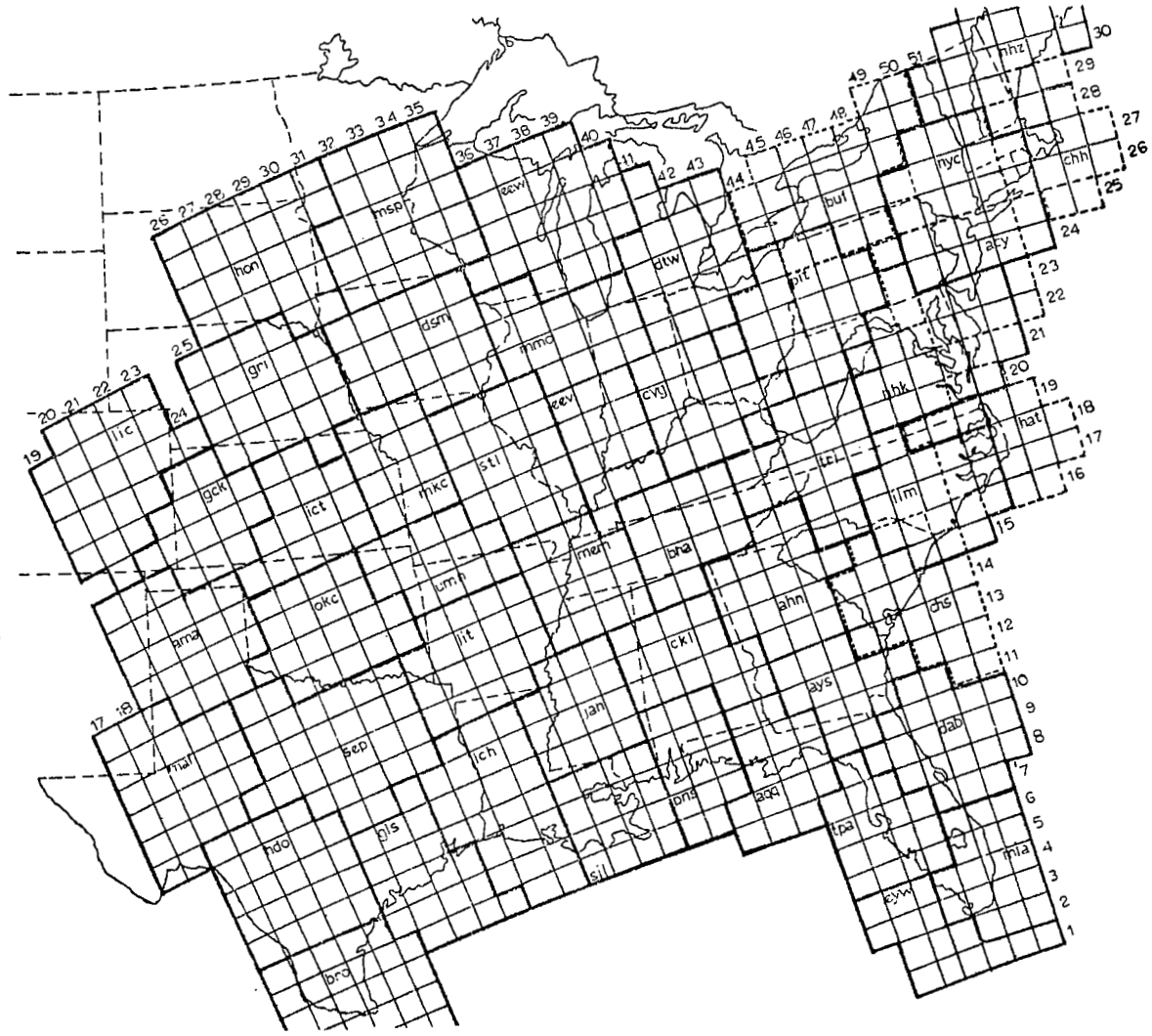

Fig. 3. Manually Digitized Radar (MDR) grid network.

assigning to each particular MDR block the highest MDR value reported within that block from any of the three 1-h periods centered about each AVE time. The composite charts were then used to separate the convective and nonconvective areas.

3. SYNOPTIC CONDITIONS

At the beginning of AVE II (1200 GMT, 11 May 1974), the synoptic situation consisted of a large mass of polar air pushing southeastward out of the Great Plains, preceded by an active cold front extending southwestward from an intense low pressure center in northeastern Minnesota. Ahead of the cold front, moist subtropical air was flowing northward into the Mississippi Valley, while a cold, polar air mass over New England was receding to the northeast. A warm sector cyclone was centered south of Louisiana. Surface and 500-mb charts are shown in Fig. 4 for 1500 GMT, 11 May 1974, and in Fig. 5 for 0900 GMT, 12 May 1974.

During the course of the experiment, the cyclone center in the midwest moved to Lake Superior, while the associated frontal system occluded further and moved eastward into the Appalachian Mountains. The southern portion of the cold front moved southward into the lower Mississippi Valley region, but was undergoing frontolysis by the end of the experiment. The Gulf coast cyclone moved northeastward across southeastern Louisiana to northwestern South Carolina.

Precipitation associated with the synoptic features was widespread and intense at times. Showers and heavy thunderstorms were occurring in southern Louisiana and Mississippi in association with the Gulf cyclone at the beginning of AVE II. A broad band of showers stretched northward ahead of the cold front into the lower Great Lakes region, where heavier storms were present ahead of the surface warm front's position. Stratiform rain occurred over the upper Great Lakes area around the occluding low center. The pattern of precipitation moved eastward during the remainder of AVE II, and the precipitation became less intense, gradually becoming stratiform rain except in the southeastern states where heavy convection continued.

In addition to the major synoptic features, two mesoscale systems affected portions of the AVE II grid. Post-frontal heavy thunderstorms broke out in South Dakota and Minnesota around 2100 GMT on 11 May 1974 in response to the passage of an upper level trough. In the southeast, a squall line with severe thunderstorms formed at 0600 GMT on

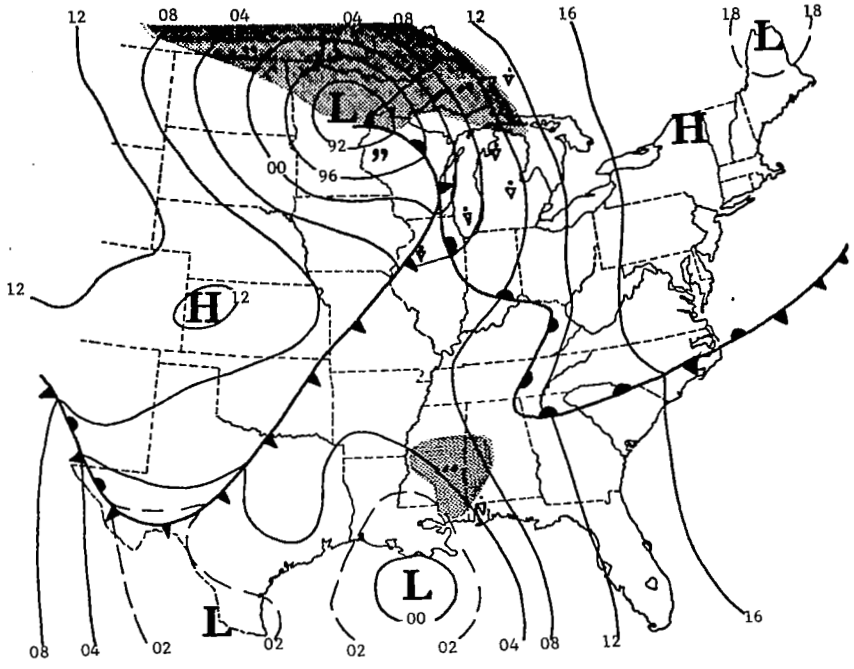

(a) Surface

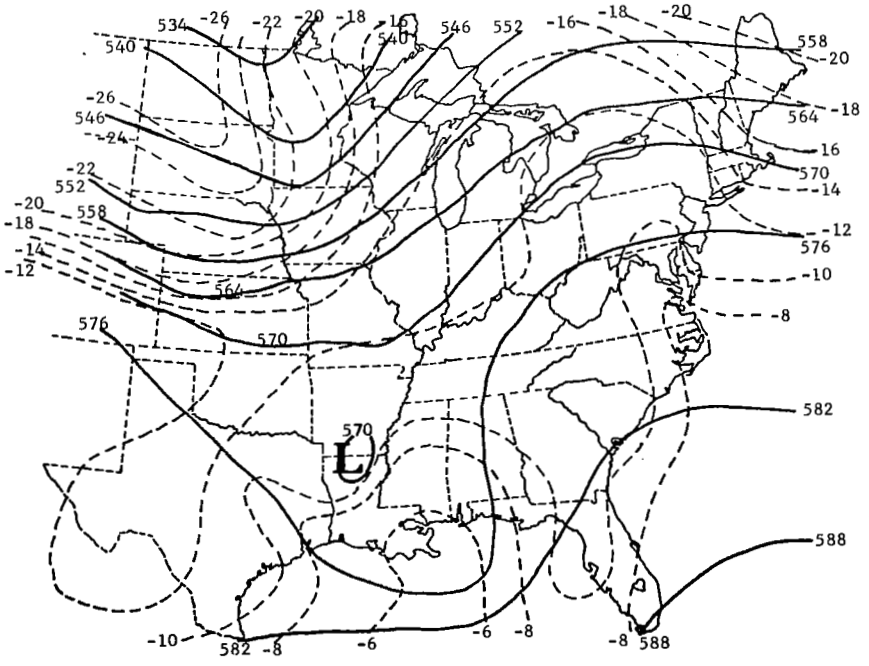

(b) 500 mb

Fig. 4. Synoptic charts for 1500 GMT, 11 May 1974.

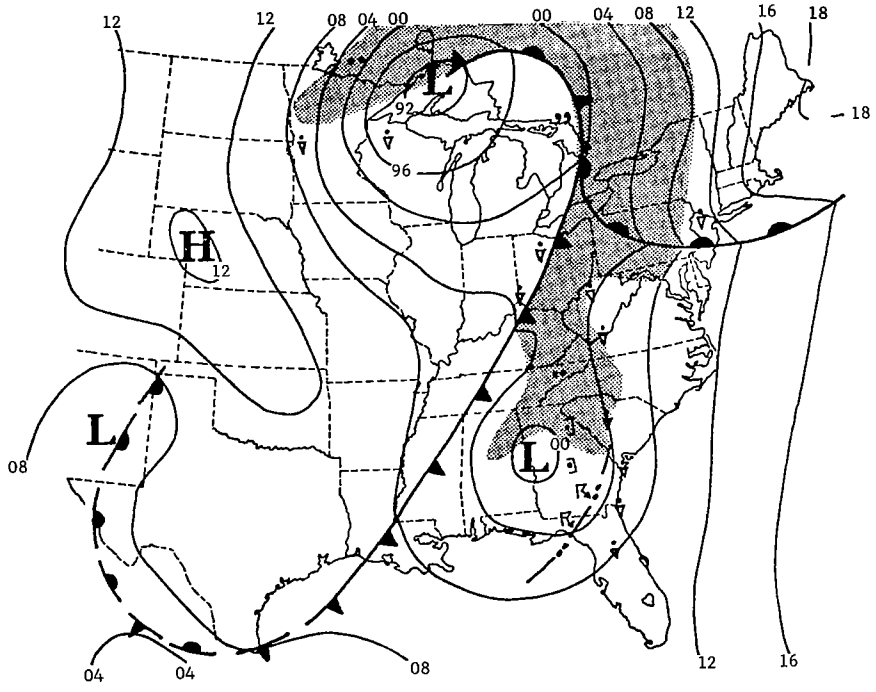

(a) Surface

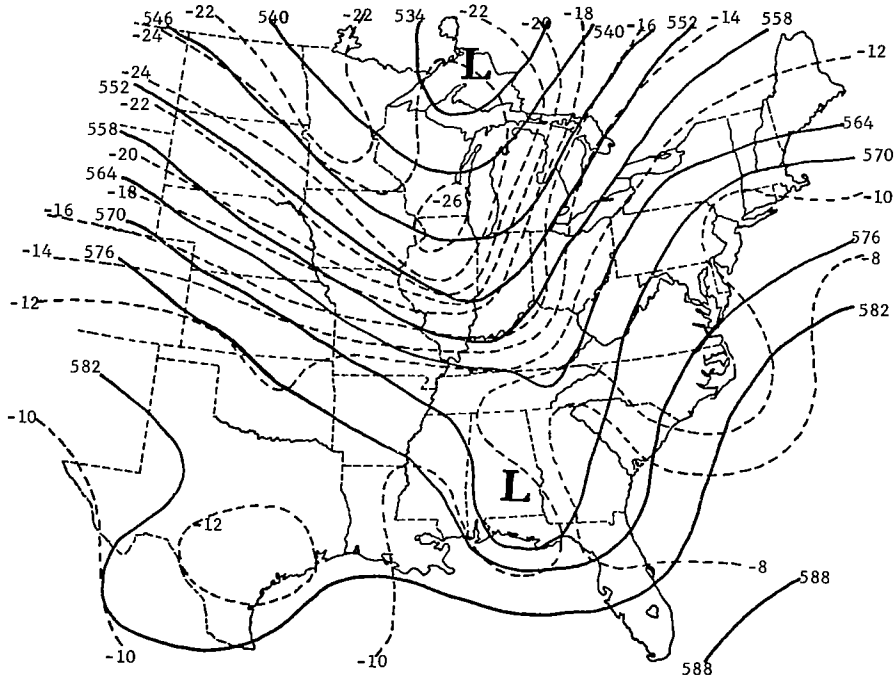

(b) 500 mb

Fig. 5. Synoptic charts for 0900 GMT, 12 May 1974.

12 May 1974, and moved through northern Florida, eastern Georgia, and southeastern South Carolina.

The synoptic situation during AVE IV provided a sharp contrast to that prevailing during AVE II. Whereas the situation in AVE II was strongly baroclinic, the systems in AVE IV were relatively weak with mostly zonal flow in the upper levels; nevertheless, two major squall lines and numerous other areas of precipitation occurred at various times during the course of the experiment. Figures 6 and 7 show surface and 500-mb maps for 0000 GMT, 24 April 1975, and 1200 GMT, 25 April 1975, the beginning and ending times of the experiment, respectively.

The synoptic situation at the beginning of AVE IV (0000 GMT, 24 April 1975) consisted of a mass of polar air moving slowly southeastward out of the north central states into warm, moist subtropical air lying over most of the eastern United States. A different mass of polar air was retreating northeastward out of the New England and the middle Atlantic states. Ahead of the polar air mass in the north central and western states lay a weak front associated with minor low pressure centers in northeastern Michigan, south central Kansas, and in north central Mexico. From the low in Michigan, a stationary front extended southeastward across Pennsylvania into the Atlantic. By the end of AVE IV (1200 GMT, 25 April 1975), the polar air mass in the north central states had pushed eastward to the Atlantic in the northern states, but had made little progress in moving southward. A cold front lay south of the New England coast and across Maryland to a frontal wave in northern Kentucky, and from there southwestward into southwest Texas where the front became stationary.

Two major outbreaks of severe weather occurred during AVE IV. Both outbreaks initially were present along the frontal region and moved eastward away from the front while slowly degenerating. The first outbreak of severe weather was already in progress at the beginning of AVE IV. A post-frontal area of severe storms was present in western Kansas and central Nebraska, while a pre-frontal squall line lay across northern Missouri. Maximum tops along this squall line were reported by radar at 60,000 ft.

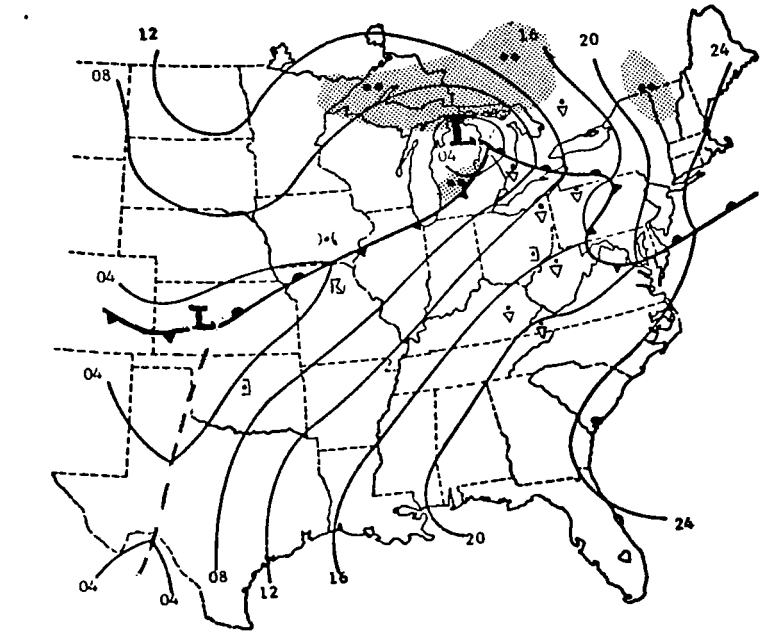

(a) Surface

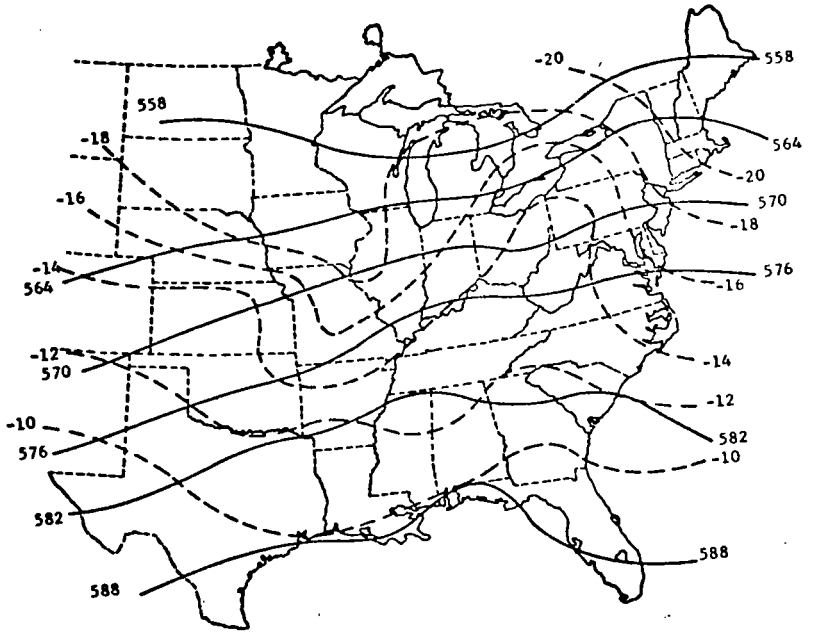

(b) 500 mb

Fig. 6. Synoptic charts for 0000 GMT, 24 April 1975.

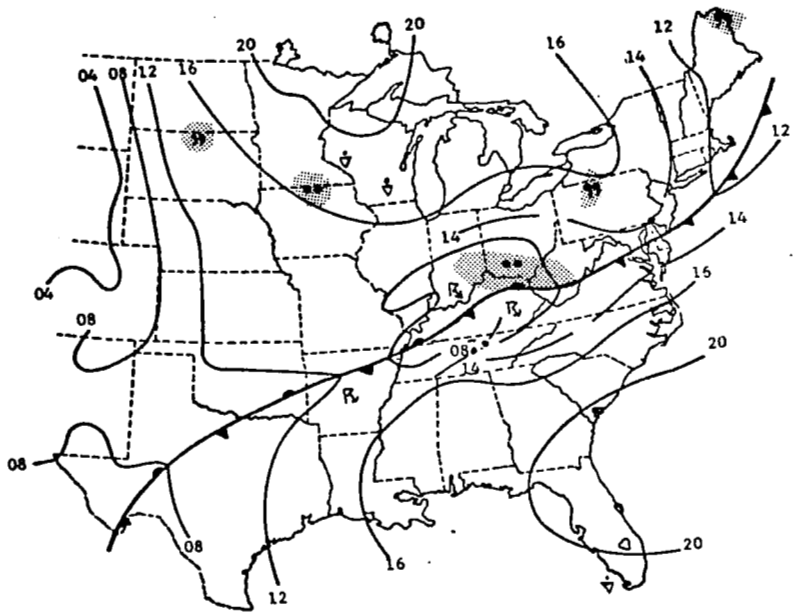

(a) Surface

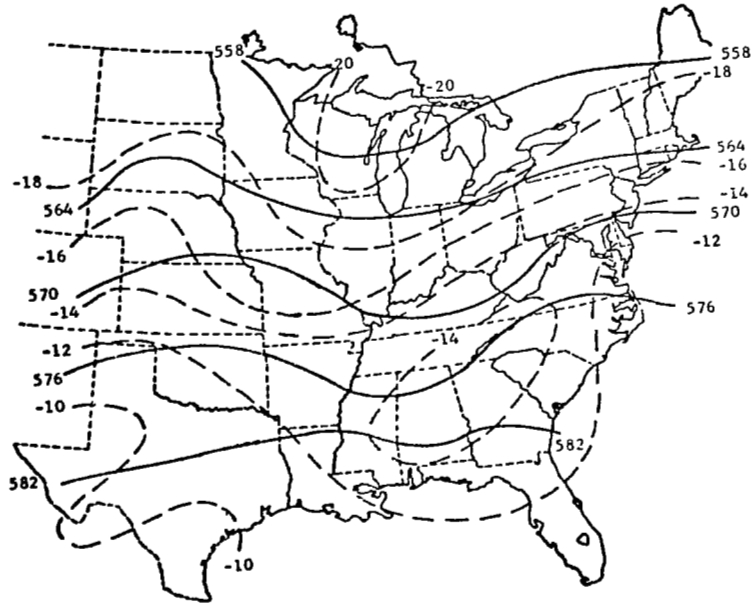

(b) 500 mb

Fig. 7. Synoptic charts for 1200 GMT, 25 April 1975.

The storm system moved eastward away from the front during the next 15 h and weakened considerably, but gained strength again during the following 6 h and produced a squall line that at 2100 GMT stretched from southeastern Kentucky into north central Tennessee. By 0000 GMT, the remains of this system contained a broad area of stratiform rain with embedded thundershowers covering the southern Appalachians.

Concurrent with the renewed strengthening of the first storm system, a new area of heavy thunderstorms began building at 1800 GMT in eastern Kansas near the position of the surface low. By 0000 GMT, 25 April 1975, a squall line containing severe storms stretched from northwestern Arkansas into eastern Oklahoma with other heavy storms stretching northward into central Missouri. The squall line continued to move eastward and develop with maximum intensity occurring around 0600 GMT. By 1200 GMT, 25 April 1975, the end of the AVE IV experiment, the system existed as an unbroken line of heavy thunderstorms from southeastern Kentucky curving southwestward through northwestern Alabama into southeastern Arkansas. Maximum tops as reported by radar along the squall line were still occasionally above 50,000 ft.

4. STRATIFICATION OF DATA

The fact that there were major differences between the synoptic conditions prevailing during AVE II and AVE IV has been noted previously; accordingly, differences of the gradient patterns and distributions should be expected when comparing the two experiments. In order to study these differences, the data from each of the experiments were treated separately. Since improved and more efficient methods of working with the data were developed as the research progressed, a more extensive investigation of the gradients was performed on AVE IV than on AVE II.

Gradients were first considered without regard to convective areas and were calculated for grid points over distances of 315, 630, and 944 km. Cumulative frequency distributions of the computed quantities for each of the three distances were determined for both AVE II and AVE IV.

In an effort to determine differences in gradients observed in convective and nonconvective areas, Manually Digitized Radar data were used to define convective areas. Overlays of the composite MDR charts were placed over the computer-generated parameter grid, and any parameter grid point within one-half grid spacing of an MDR block containing a value of 4 or greater was considered as a convective area.

Since distances of 630 km and 944 km were so much larger than the storm areas, no attempt was made to classify the horizontal gradients on scales this large into either convective or nonconvective areas. Even when considering the gradients on a scale as small as 315 km, it should be emphasized that for a particular grid point, some of the gradients had to be calculated using one or more grid points outside of the convective region.

Following the designation of each grid point as being in either a convective or nonconvective area, cumulative frequency distributions and the determination of several statistical parameters were made for the data in convective and nonconvective areas over all nine times in each experiment. For AVE IV, the means of the gradients over

convective and nonconvective areas were determined separately for each time, allowing one to see how the mean gradient values changed over these areas. The areas on the grid were also subdivided into four categories according to the strength of the convection as determined from the radar data. These categories and the corresponding MDR values are as follows.

Precipitation category	MDR values
Weak or no precipitation	0,1
Moderate precipitation or less	0,1,2,3
Strong or intense precipitation	4,5,6,7,8,9
Intense precipitation	8,9

Statistical studies of the gradients of the meteorological parameters were made then for each of these categories. It should be noted that the category labelled "strong or intense convection" is the same category as that of the "convective" areas defined previously.

In an effort to concentrate on how the gradients change as storms move into (or develop in) an area, the horizontal gradients at grid points which were initially in nonconvective regions, but were in convective regions in the succeeding time period, were classified as "prestorm" gradients. Similarly, grid points which had been in convective areas, but were in nonconvective areas a time period later, were classified as "poststorm" points. The mean of the horizontal gradients in such prestorm or poststorm areas was then compared with the mean over the same grid points in the corresponding storm areas a time period later, or earlier, than the respective prestorm or poststorm time. For the AVE II data, only limited areas and 850- and 500-mb levels were considered for this study, and the times ran consecutively from the beginning of AVE II (1200 GMT, 11 May 1974) through 0300 GMT, 12 May 1974, at which time most of the areas of convection were dissipating rapidly.

For the AVE IV data a more extensive investigation involving the change of intensity of storm areas for all nine time periods and four pressure levels was performed. The changes of intensity of precipitation were subdivided into the following divisions.

Development			Dissipation		
Prestorm		Storm	Storm		Poststorm
MDR = 0,1	to	MDR ≥ 2	MDR ≥ 2	to	MDR = 0,1
MDR = 0,1	to	MDR ≥ 4	MDR ≥ 4	to	MDR = 0,1
MDR ≤ 3	to	MDR ≥ 4	MDR ≥ 4	to	MDR ≤ 3
4 ≤ MDR ≤ 7	to	MDR = 8,9	MDR = 8,9	to	4 ≤ MDR ≤ 7

The third category in this division corresponds to the prestorm or poststorm areas used in analyzing AVE II data.

In an attempt to determine the gradients observed in convective and nonconvective areas under the influence of a similar synoptic pattern, two regions in AVE II were selected for more detailed study. Only 850- and 500-mb levels for the first six times (through 0300 GMT, 12 May 1974) were considered. These regions, located in the midwest and the southeast, were under distinctly different synoptic situations. The analysis method applied to these regions was identical to the method applied to the whole grid. Means of the gradients of the meteorological parameters for convective and nonconvective areas were computed for each region for the group of six times, as well as for each time separately. Means over the prestorm and poststorm areas and their respective storm areas within each region also were considered.

In order to study the changes in the gradients of the meteorological parameters occurring during the life cycle of a squall line, the means of the gradients over both squall lines in AVE IV were computed. Time continuities of particular gradient patterns relative to nearby convective areas also were examined

using the analyzed gradient fields for the AVE IV squall lines as well as for the AVE II convective areas.

5. COMPUTATIONAL PROCEDURES

a. Gridding of rawinsonde data

Fields of geopotential height, temperature, wind speed, and mixing ratio were prepared at several pressure levels by using an objective weighted-averaging interpolative scheme developed by Barnes (1964). The method, which assumes that an atmospheric variable can be represented by a Fourier integral representation, interpolated the rawinsonde data processed at 25-mb intervals to a grid (Fig. 8) with approximately 158-km spacing between grid points. This gives the maximum resolution possible for the existing rawinsonde network (Barr et al., 1971). In both AVE II and AVE IV, the

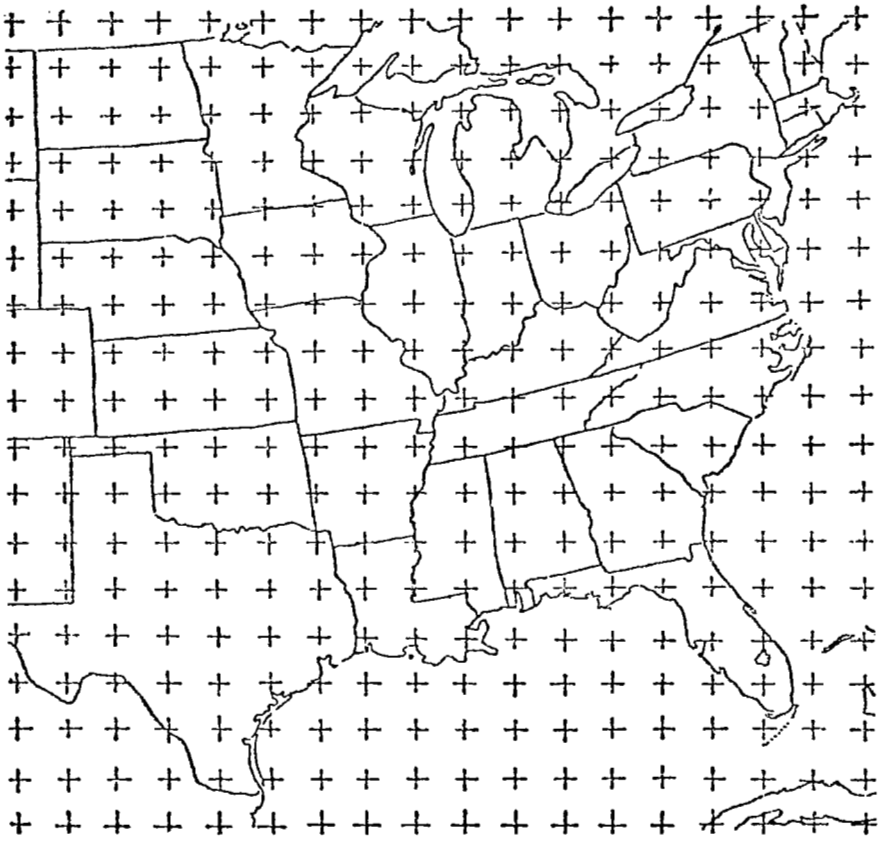

Fig. 8. Grid used for numerical computations.

data from each rawinsonde station were allowed to influence grid points within a radius of three grid intervals. The minimum number of iterations needed with the Barnes method to provide an adequate data field having the desired resolution was four.

b. Gradients

The field of any scalar Q(x,y) can be represented by a set of lines along which Q is constant. The horizontal ascendant vector, $\vec{\nabla}_n Q$, may be written as

$$\vec{\nabla}_n Q = \vec{n}\left(\frac{dQ}{dn}\right) = \hat{i}\left(\frac{\partial Q}{\partial x}\right) + \hat{j}\left(\frac{\partial Q}{\partial y}\right), \quad (1)$$

where $\vec{n}$ is normal to the isolines of Q and in the direction of increasing Q. The magnitude of this vector is given by

$$|\vec{\nabla}_n Q| = \left[\left(\frac{\partial Q}{\partial x}\right)^2 + \left(\frac{\partial Q}{\partial y}\right)^2\right]^{1/2}. \quad (2)$$

Following the convention of Saucier (1955), the word "gradient" will refer hereafter only to the magnitude of the ascendant vector.

The centered finite difference approximation for the gradient at any grid point (i,j) can be calculated by the formula:

$$|\vec{\nabla}_n Q|_{ij} = \frac{\sqrt{(q_{i+1} - q_{i-1})^2 + (q_{j+1} - q_{j-1})^2}}{\Delta s} \quad (3)$$

where Δs is the spacing between grid points used in the computation. In this case, Δs represents 315 km since the spacing between adjacent grid points is approximately 157.5 km. Gradients over the distances of 630 km and 944 km also were calculated by considering the values of the parameters at grid points of i + 2, i - 2, j + 2, j - 2, and i + 3, i - 3, j + 3, and j - 3, respectively. Gradients hereafter will be expressed as differentials (not divided by Δs), or as changes per unit distance (divided by Δs).

Geopotential height, temperature, and wind speed gradients were calculated at 850, 700, 500, and 200 mb for each of the three different distances, and for all times in AVE II and AVE IV. Mixing ratio gradients were similarly computed, but only for the 850-, 700-, and 500-mb levels. The solid line in Fig. 9

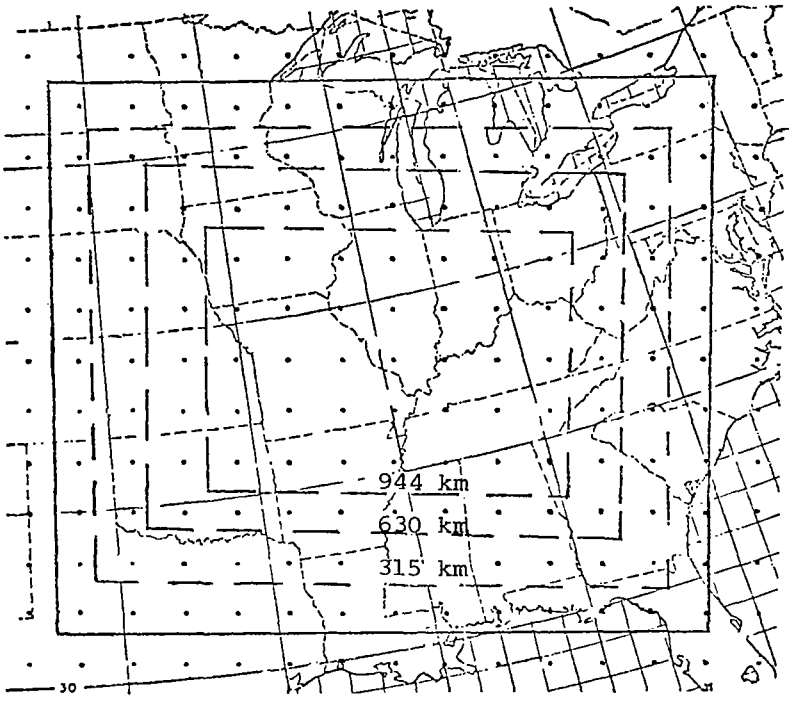

Fig. 9. Boundaries encompassing grid points at which gradients over 315, 630, and 944 km were computed.

represents the outer boundary of grid points used in computing the gradients observed for each of the three distances. For each time, there were 99 grid points for the 315-km distance, 63 for the 630-km distance, and 35 for the 944-km distance.

c. Statistical parameters

Several statistical techniques were employed in evaluating the data. These included the use of cumulative frequency distributions, sample mean and median as measures of central tendency, and the standard deviation, coefficient of variation, and skewness as indicators of the dispersion and variability of the data. In preparing cumulative frequency distributions, the data were first grouped into 20 consecutive, equally-divided class intervals, and the cumulative percent up to the upper limit of each interval was

determined. Such distributions can be plotted on probability graph paper which can be used to determine how well a given distribution can be fit to a normal distribution.

Used as a measure of central tendency of the data, the mean is the arithmetic average of all the values. The median is the [(n + 1)/2]th observation when the values are arranged in order of magnitude. Since the 50th percentile on a cumulative frequency distribution represents the median, median values in this study were approximated by using an interpolative method as described by Ostle and Mensing (1975).

The most familiar measure of the variability of data is the standard deviation, and is defined by

$$s = \left[\sum_{i=1}^{N} (x_i - \bar{x})^2 / N \right]^{1/2}, \qquad (4)$$

where x_i represents the ith observation of a set of numbers, $\bar{x}$ represents the mean, and N is the total number of observations. The coefficient of variation, CV, is a measure of the dispersion of the data, and is useful in comparing series of data that are measured in different units. The variation is expressed as a fraction of the mean and is defined as $CV = s/\bar{x}$. Skewness, a measure of the asymmetry of a distribution, was not calculated directly, but the sign of the skewness was indicated by the relative magnitude of the mean and median values. In symmetric distributions, the median and mean coincide. In cases where the median is less than the mean, positive skewness is indicated, and in cases where the reverse is true, there is negative skewness.

6. RESULTS

a. Gradients

Statistical approaches were used to delineate differences in the gradients of the meteorological variables in convective and nonconvective areas. In each case, the mean, median, standard deviation, and coefficient of variation were computed for each set of data and cumulative frequency distributions prepared. The results are presented in both tabular and graphical form. Since the grid areas for AVE II and AVE IV were exactly the same size, there were data from 891, 567, and 315 grid points when the gradients were computed over 315, 630, and 944 km, respectively.

1) Convective areas

Table 1 contains values of statistical parameters computed for the gradients in convective areas of AVE II and AVE IV. Meteorological variables and the pressure levels are listed on the left and the statistical parameters are listed along the top. In all cases, the gradients were computed over 315-km distances and there were 196 grid points considered in AVE II and 167 grid points in AVE IV.

Geopotential height gradients in the convective areas in both experiments increased with height, and the standard deviations were approximately 30-50% as large as the mean. In AVE II, the distributions were skewed to the right (positive skewness), but the distributions in AVE IV were skewed to the left (negative skewness).

Mean temperature gradients in the convective areas were not very large, being in both experiments at all pressure levels less than 3.5°C/315 km. In AVE IV, the mean horizontal gradients decreased as higher levels in the atmosphere were considered; whereas, in AVE II no general trend was established. Positive skewness of the distributions was indicated at all pressure levels in both experiments.

Wind speed gradients in both experiments exhibited positive skewness. In AVE II, gradients became stronger at successively

Table 1. Selected statistical parameters of gradients in convective areas.

Parameter	AVE II				AVE IV			
	Median	Mean	Standard Deviation	Coefficient of Variation	Median	Mean	Standard Deviation	Coefficient of Variation
Geopotential Height			(m/315 km)				(m/315 km)	
850 mb	42.9	45.3	20.4	.45	35.8	34.7	15.8	.45
700 mb	51.7	54.0	24.6	.46	47.0	46.2	15.0	.32
500 mb	58.5	64.4	33.1	.51	68.2	67.8	14.4	.21
200 mb	85.6	94.8	43.6	.46	101.1	100.9	30.7	.30
Temperature			(°C/315 km)				(°C/315 km)	
850 mb	2.8	2.9	1.6	.55	3.3	3.4	1.9	.55
700 mb	2.1	2.3	1.3	.57	2.6	2.7	1.1	.41
500 mb	1.8	2.4	2.0	.83	2.1	2.2	1.2	.55
200 mb	2.4	3.1	2.4	.77	2.1	2.2	1.2	.55
Wind Speed			(m/sec/315 km)				(m/sec/315 km)	
850 mb	6.4	7.2	4.2	.58	8.4	8.5	4.3	.51
700 mb	7.4	7.5	3.5	.47	6.2	6.5	3.4	.52
500 mb	8.1	8.6	4.7	.55	6.2	6.7	3.6	.54
200 mb	10.9	11.5	6.4	.56	8.5	9.1	5.6	.62
Mixing Ratio			(g/kg/315 km)				(g/kg/315 km)	
850 mb	2.8	3.0	2.0	.67	2.4	2.8	1.8	.64
700 mb	2.0	2.4	1.4	.58	2.3	2.3	1.2	.52
500 mb	1.2	1.3	0.8	.62	0.8	0.9	0.6	.67

higher levels, but in AVE IV the strongest gradients occurred at 850 and 200 mb.

Mixing ratio gradients were slightly larger in AVE II than in AVE IV. In both cases, the horizontal gradients decreased as successively higher levels were considered. Large variability was present in the gradients at all levels.

Overall, mean gradients over convective areas in both AVE II and AVE IV were similar in magnitude. Virtually all the distributions were positively skewed to some degree, and in most cases, the standard deviations of the gradients were about half as large as the means, which indicated a wide range in the value of the gradients of each of the parameters.

2) Nonconvective areas

Table 2 shows values of statistical parameters computed for gradients in nonconvective areas of AVE II and AVE IV. Gradients were computed over 315-km distances in all cases; there were 695 grid points in AVE II and 724 grid points in AVE IV.

The distributions of geopotential height gradients in nonconvective areas were positively skewed in AVE II, and at 850 and 700 mb in AVE IV. While in AVE II the standard deviation at all levels was approximately half as large as the mean, in AVE IV the ratio of standard deviation to mean decreased with height, i.e., the coefficient of variation decreased as higher levels were considered. At all levels, the mean gradients were larger in AVE II than in AVE IV, indicating that the intensity of the general synoptic situation was stronger in AVE II than in AVE IV.

Mean temperature gradients at all levels in nonconvective areas of AVE II were larger than the gradients at corresponding levels of AVE IV. Above 700 mb in AVE II, the standard deviations and coefficients of variation all increased with height, indicating that the variability of the gradients, as expressed by the standard deviations, was also increasing with height. In AVE IV, no general relationship such as this held true, although the mean gradients decreased with height. The fact that mean temperature gradients in AVE II increased with height while those in AVE IV decreased

Table 2. Selected statistical parameters of gradients in nonconvective areas.

Parameter	AVE II				AVE IV			
	Median	Mean	Standard Deviation	Coefficient of Variation	Median	Mean	Standard Deviation	Coefficient of Variation
Geopotential Height			(m/315 km)				(m/315 km)	
850 mb	36.5	40.0	22.0	.55	23.1	26.6	16.7	.63
700 mb	51.6	54.2	27.3	.50	33.5	35.5	15.0	.42
500 mb	72.3	81.0	43.7	.54	54.0	53.9	16.6	.31
200 mb	102.9	107.4	56.4	.53	94.6	94.7	28.4	.30
Temperature			(°C/315 km)				(°C/315 km)	
850 mb	3.5	3.6	2.0	.56	2.9	3.3	1.9	.58
700 mb	3.7	3.7	2.0	.54	2.6	2.7	1.2	.44
500 mb	2.6	3.6	2.7	.75	2.1	2.2	1.1	.50
200 mb	2.7	4.1	3.5	.85	1.8	2.0	1.2	.60
Wind Speed			(m/sec/315 km)				(m/sec/315 km)	
850 mb	6.0	6.4	3.5	.55	5.2	5.8	3.5	.60
700 mb	6.1	6.8	3.7	.54	6.2	6.8	3.9	.57
500 mb	9.3	9.9	5.3	.54	6.4	6.9	3.8	.55
200 mb	11.7	13.0	7.9	.61	7.4	8.2	5.1	.62
Mixing Ratio			(g/kg/315 km)				(g/kg/315 km)	
850 mb	2.5	3.1	2.2	.71	2.3	2.6	1.6	.62
700 mb	2.0	2.3	1.4	.61	1.8	1.9	1.1	.58
500 mb	0.7	0.9	0.7	.78	0.6	0.8	0.6	.75

with height was another indication of the differences in the weather systems in the two experiments.

Positive skewness was inherent in the wind speed gradient distributions at all levels in both experiments. The mean of the gradients increased with height in both experiments, and the standard deviation was roughly one-half the magnitude of the mean gradient at each level.

Mixing ratio gradients in the nonconvective areas of AVE II at each level were larger than the gradients at corresponding levels in AVE IV. Large variability in the gradients was present as evidenced by the large coefficients of variation.

As was the case for convective areas, the magnitudes of the means of the gradients in nonconvective areas of AVE II and AVE IV were similar. The fact that the mean gradients in AVE II were somewhat larger than those in AVE IV has implications as to the strength of the general synoptic situation. In general, the distributions were positively skewed and had a standard deviation half as large as the mean at each level.

3) Combined areas

Statistical information about the gradients in AVE II and AVE IV over distances of 315 km without regard to convection is given in Table 3. Since the information is simply a compilation of the information given previously, little comment is needed. Gradients in AVE II tended to be larger and, with the exception of wind speed, more variable than those in AVE IV. Of the pressure levels studied, 700-mb gradients appeared to be less variable than those at other pressure levels.

Tables 4 and 5 contain statistical information about gradients computed over 315-, 630-, and 944-km distances in AVE II and in AVE IV, respectively. To enhance comparisons, the gradients in these tables have been divided by their respective distances to yield gradients in terms of unit kilometer distances.

Geopotential height gradients at 850, 700, and 500 mb became progressively smaller as gradients over 315-, 630-, and 944-km distances were computed for AVE II. At 200 mb in AVE II, and at

Table 3. Selected statistical parameters of gradients without regard to convection.

Parameter	AVE II				AVE IV			
	Median	Mean	Standard Deviation	Coefficient of Variation	Median	Mean	Standard Deviation	Coefficient of Variation
Geopotential Height			(m/315 km)				(m/315 km)	
850 mb	38.1	41.2	21.8	.53	25.6	28.1	16.9	.60
700 mb	51.6	54.2	26.8	.49	35.7	37.5	15.5	.41
500 mb	67.4	77.3	42.2	.55	57.7	56.5	17.1	.30
200 mb	97.5	104.6	54.1	.52	95.7	95.9	29.0	.30
Temperature			(°C/315 km)				(°C/315 km)	
850 mb	3.3	3.4	1.9	.56	3.0	3.3	1.9	.57
700 mb	3.3	3.4	2.0	.59	2.6	2.7	1.2	.44
500 mb	2.4	3.4	2.6	.76	2.1	2.2	1.1	.50
200 mb	2.6	3.8	3.3	.87	1.9	2.0	1.2	.60
Wind Speed			(m/sec/315 km)				(m/sec/315 km)	
850 mb	6.1	6.6	3.7	.56	5.7	6.3	3.8	.60
700 mb	6.3	6.9	3.6	.52	6.2	6.7	3.8	.57
500 mb	9.0	9.6	5.2	.54	6.3	6.8	3.8	.56
200 mb	11.5	12.7	7.6	.60	7.5	8.4	5.2	.62
Mixing Ratio			(g/kg/315 km)				(g/kg/315 km)	
850 mb	2.6	3.1	2.2	.71	2.3	2.6	1.6	.62
700 mb	2.0	2.3	1.4	.61	1.9	2.0	1.1	.55
500 mb	0.7	1.0	0.7	.70	0.7	0.8	0.6	.75

Table 4. Selected statistical parameters for different gradient distances in AVE II.

Parameter	315 km distance--891 grid points				630 km distance--567 grid points				944 km distance--315 grid points			
	Median	Mean	Standard Deviation	Coefficient of Variation	Median	Mean	Standard Deviation	Coefficient of Variation	Median	Mean	Standard Deviation	Coefficient of Variation
Geopotential Height			(m/km)				(m/km)				(m/km)	
850 mb	.121	.131	.0693	.529	.105	.115	.0572	.498	.101	.100	.0472	.473
700 mb	.164	.172	.0851	.494	.156	.159	.0729	.458	.149	.148	.0629	.424
500 mb	.214	.246	.134	.546	.245	.244	.113	.484	.254	.238	.0993	.417
200 mb	.309	.332	.172	.517	.336	.336	.140	.418	.338	.334	.109	.327
Temperature			(°C/km)				(°C/km)				(°C/km)	
850 mb	.0104	.0108	.00604	.558	.00944	.00953	.00461	.483	.00925	.00879	.00371	.422
700 mb	.0104	.0108	.00635	.588	.0103	.0103	.00508	.492	.0109	.00985	.00445	.452
500 mb	.00762	.0108	.00826	.765	.00804	.0102	.00683	.672	.0101	.00995	.00498	.500
200 mb	.00830	.0121	.0105	.868	.00777	.0110	.00842	.768	.00843	.00953	.00604	.633
Wind Speed			(m/sec/km)				(m/sec/km)				(m/sec/km)	
850 mb	.0194	.0210	.0118	.561	.0137	.0145	.00699	.484	.00963	.00995	.00498	.500
700 mb	.0202	.0219	.0114	.522	.0164	.0167	.00826	.495	.0119	.0121	.00561	.465
500 mb	.0285	.0305	.0165	.542	.0237	.0245	.0129	.526	.0196	.0192	.00826	.431
200 mb	.0366	.0403	.0241	.598	.0311	.0327	.0165	.505	.0231	.0244	.0119	.487
Mixing Ratio			(g/kg/km)				(g/kg/km)				(g/kg/km)	
850 mb	.00812	.00985	.00699	.710	.00683	.00715	.00429	.600	.00574	.00561	.00275	.491
700 mb	.00621	.00731	.00445	.609	.00486	.00524	.00286	.545	.00413	.00413	.00191	.462
500 mb	.00238	.00318	.00222	.700	.00215	.00238	.00159	.667	.00202	.00191	.00106	.556

Table 5. Selected statistical parameters for different gradient distances in AVE IV.

Parameter	315 km distance--891 grid points				630 km distance--567 grid points				944 km distance--315 grid points			
	Median	Mean	Standard Deviation	Coefficient of Variation	Median	Mean	Standard Deviation	Coefficient of Variation	Median	Mean	Standard Deviation	Coefficient of Variation
Geopotential Height			(m/km)				(m/km)				(m/km)	
850 mb	.0812	.0893	.0536	.600	.0923	.0895	.0500	.559	.0784	.0749	.0340	.454
700 mb	.113	.119	.0493	.414	.124	.124	.0373	.301	.0951	.0946	.0224	.237
500 mb	.183	.179	.0542	.303	.182	.187	.0350	.187	.141	.138	.0193	.140
200 mb	.304	.304	.0920	.303	.316	.313	.0665	.212	.228	.225	.0466	.207
Temperature			(°C/km)				(°C/km)				(°C/km)	
850 mb	.00943	.0105	.00603	.574	.00967	.00971	.00448	.461	.00576	.00584	.00254	.435
700 mb	.00813	.00841	.00378	.449	.00765	.00778	.00273	.351	.00551	.00555	.00163	.294
500 mb	.00654	.00698	.00352	.504	.00652	.00641	.00316	.493	.00457	.00450	.00237	.527
200 mb	.00594	.00644	.00378	.587	.00511	.00540	.00286	.530	.00418	.00423	.00209	.494
Wind Speed			(m/sec/km)				(m/sec/km)				(m/sec/km)	
850 mb	.0179	.0201	.0121	.602	.0158	.0166	.00921	.555	.0139	.0140	.00627	.448
700 mb	.0197	.0214	.0121	.565	.0155	.0170	.00890	.524	.0137	.0137	.00582	.425
500 mb	.0201	.0217	.0119	.548	.0174	.0179	.00878	.491	.0133	.0135	.00578	.428
200 mb	.0239	.0265	.0164	.619	.0193	.0202	.0120	.594	.0129	.0138	.00793	.575
Mixing Ratio			(g/kg/km)				(g/kg/km)				(g/kg/km)	
850 mb	.00730	.00825	.00511	.619	.00581	.00622	.00349	.561	.00401	.00433	.00242	.559
700 mb	.00590	.00641	.00359	.560	.00459	.00475	.00237	.499	.00328	.00345	.00172	.499
500 mb	.00210	.00254	.00178	.700	.00160	.00183	.00110	.601	.00126	.00130	.000678	.522

all levels in AVE IV, mean height gradients computed over 630-km distances were slightly larger than those computed over either 315- or 944-km distances. The gradient distributions were positively skewed for gradients computed over 315 km at all levels in AVE II, and at 850 and 700 mb in AVE IV. Over 944-km distances, the height gradient distributions at all levels in both experiments were negatively skewed, meaning there was a lack of the smaller gradient values. At all levels in both experiments, the coefficient of variation became progressively smaller as 315-, 630-, and 944-km distances were considered. This indicated that the gradients were less variable over the larger distances, as would be expected.

Temperature gradients at all levels and in both experiments decreased as the gradients were computed over progressively longer distances. Since the coefficient of variation was largest in the upper atmosphere and over the 315-km distance, it can be concluded that temperature gradients were more variable, relative to the mean, in the upper atmosphere and over short distances than elsewhere. Considering the coefficients of variation derived for each of the distributions of each of the four meteorological parameters in both experiments, the largest coefficient of variation was that of temperature gradients in AVE II at 200 mb and over a distance of 315 km. While all the distributions of temperature gradients computed over 315 km were skewed positively to some degree, many of the 944-km distributions were negatively skewed.

Mean wind speed gradients progressively decreased at all levels in both experiments as the gradients were computed over progressively longer distances. As with height and temperature gradients, the coefficient of variation became progressively smaller as the wind speed gradients were computed over 315, 630, and 944 km. This indicated that the variability of the gradients was less over longer than over shorter distances.

In all cases, mixing ratio gradients decreased as progressively longer distances were considered, and the coefficients of variation did likewise. Gradient distributions were positively skewed over

the 315- and 630-km distances, and were negatively skewed over 944-km distances at 850 and 500 mb in AVE II.

Overall, mean gradient values and the coefficients of variation at all levels tended to decrease as the gradients were computed over 315-, 630-, and 944-km distances. This should be expected since it has been shown that 30-60% of the total change observed in a synoptic-scale parameter over a 12-h period occurs within a 3-h period, and that such variability is due to subsynoptic-scale systems (Wilson and Scoggins, 1976). Presumably such systems could cause the larger variability observed in gradients computed over 315-km distances.

b. Probability of magnitudes of gradients

In order to determine the probability of the magnitudes of gradients, cumulative frequency distributions were computed without regard to convective areas for gradients over 315-, 630-, and 944-km distances, and for gradients in convective and nonconvective areas over 315-km distances. The 315-km gradients at each level were then plotted on probability graph paper for both experiments.

Cumulative frequency distributions are shown in Fig. 10a for AVE II height gradients, and in Fig. 10b for AVE IV height gradients. These frequency distributions reveal a difference in the magnitudes and distributions of the height gradients between the two experiments. For example, while 90% of the height gradients in AVE II at 850 mb were 73 m/315 km or less, the remaining 10% were distributed up to a maximum of 120 m/315 km. In AVE IV, 90% of the height gradients at 850 mb were 52 m/315 km or less, and the maximum was only 75 m/315 km.

The temperature frequency distributions plotted in Fig. 11a for AVE II and Fig. 11b for AVE IV provide the most contrast between the two experiments of any of the atmospheric variables studied. The distributions of temperature gradients in AVE II were interesting in that even though the mean temperature gradients at 500 and 200 mb were larger than those at either 700 or 850 mb, approximately 65% of the gradients at 500 and 200 mb were smaller than those at 850 or 700 mb. In contrast to the gradients in AVE II, the temperature

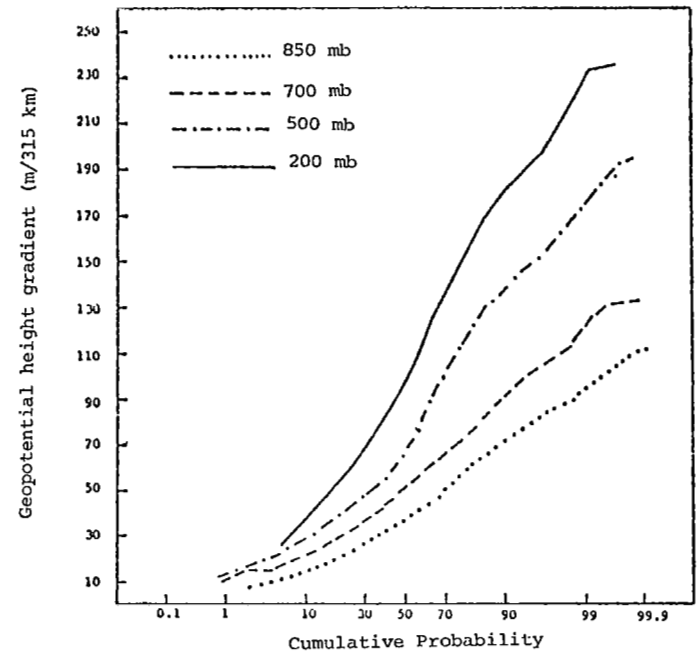

(a) AVE II

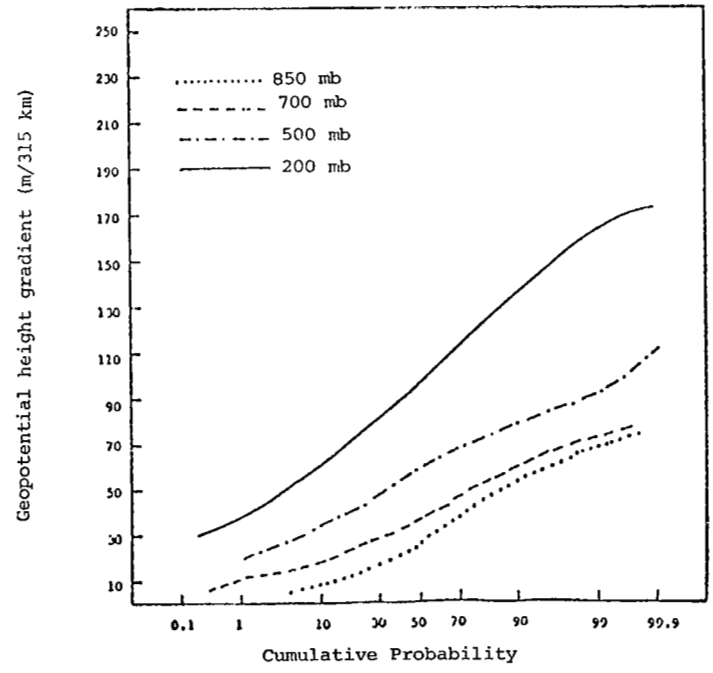

(b) AVE IV

Fig. 10. Cumulative frequency distributions of geopotential height gradients.

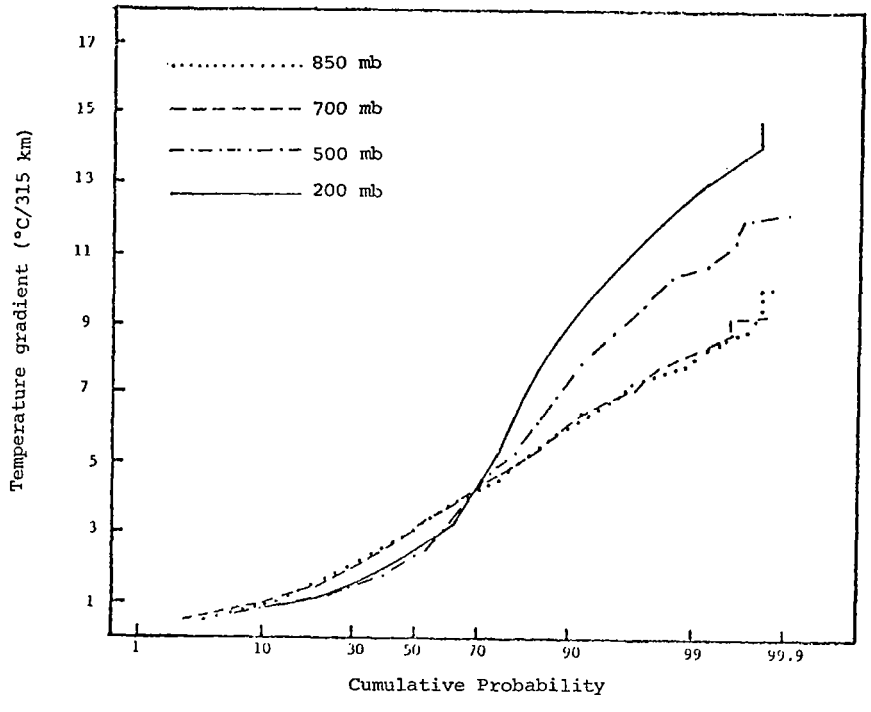

(a) AVE II

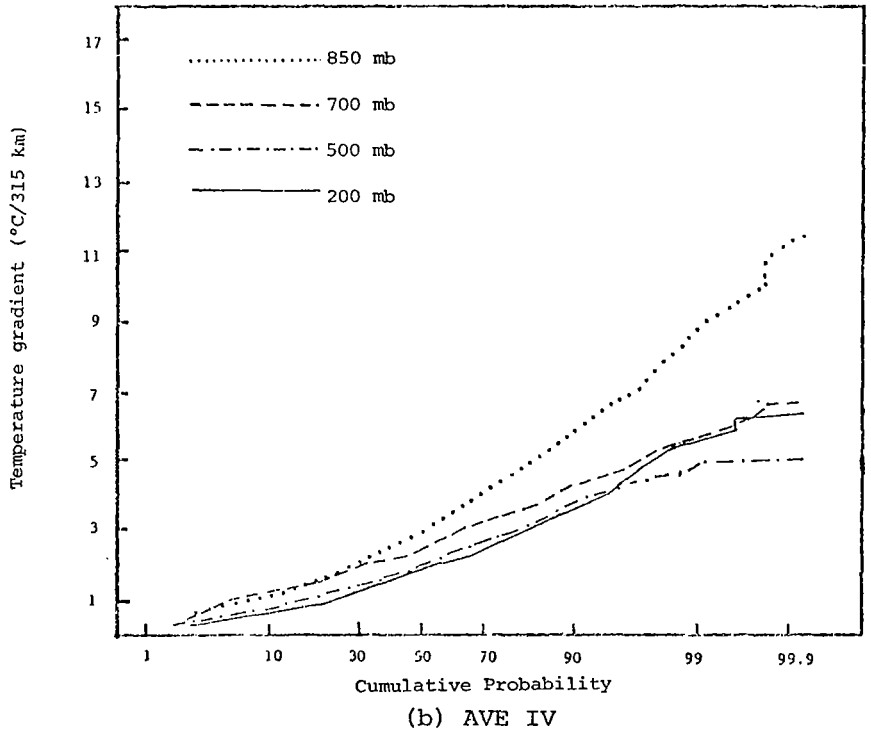

(b) AVE IV

Fig.11. Cumulative frequency distributions of temperature gradients.

gradients in AVE IV were not as irregularly distributed, and the largest mean gradients occurred at 850 mb.

Figures 12a and 12b are plots of cumulative frequency distributions of wind speed gradients for AVE II and AVE IV, respectively. Note that the cumulative frequency values of the gradients at 200 mb in AVE II are plotted on a different scale than the values for other levels. Distributions for 850 and 700 mb were nearly identical between the two experiments, but gradients at 500 and 200 mb were much larger in AVE II than in AVE IV. As an indication of the large values found in AVE II, note that 98% of the wind speed gradients at 200 mb were less than half of the maximum-reported value for that level. Such a distribution suggests the presence of a strong jet stream at some time during the period for which the data were collected, with an actual occurrence over Ohio and western New York at 0900 GMT, 12 May 1974. Wind speeds in the jet reached 100 m sec^{-1} with horizontal speed gradients of up to 70 m sec^{-1}/315 km. These extreme values were present for only one time period, but were confirmed by three separate rawinsonde stations.

Cumulative frequency distributions of mixing ratio gradients are shown in Fig. 13a for AVE II and Fig. 13b for AVE IV. The distributions are very similar for the two experiments, with a tendency toward positive skewness among all distributions. The marked decrease in the magnitudes of the horizontal gradients with respect to height should be noted. This should be expected because of the nonlinear decrease of mixing ratio with height.

Cumulative frequency distribuitons also were computed for convective and nonconvective areas in each of the two experiments. These distributions were plotted on probability graph paper for each of the meteorological variables for 850 and 500 mb in AVE II and AVE IV. Only the distributions for geopotential height gradients and wind speed gradients will be discussed.

Cumulative frequency distributions of geopotential height gradients are plotted in Figs. 14a and 14b for AVE II, and in Figs. 15a and 15b for AVE IV. In AVE II, 95% of the height gradients at 850 mb were larger in convective areas than in nonconvective areas,

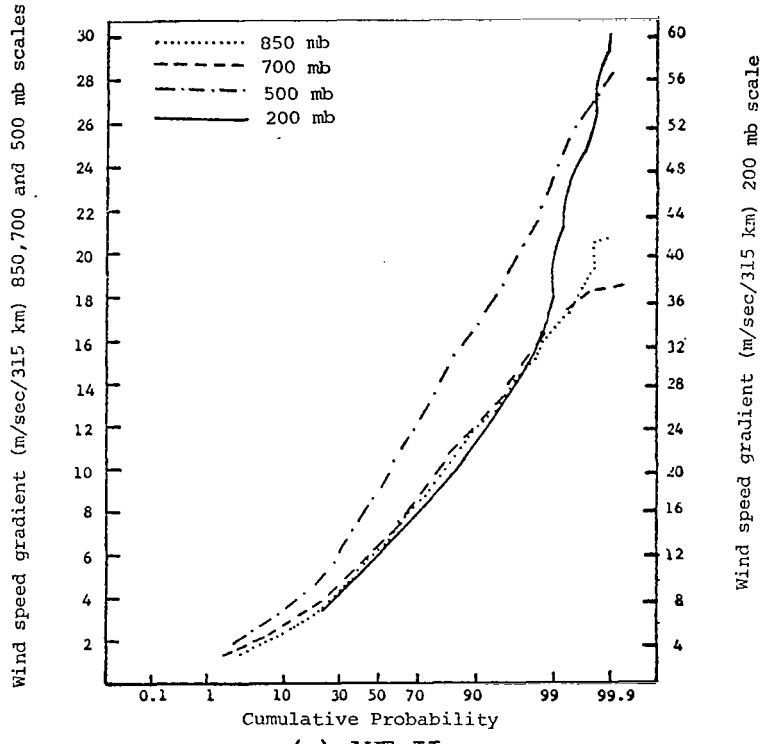

(a) AVE II

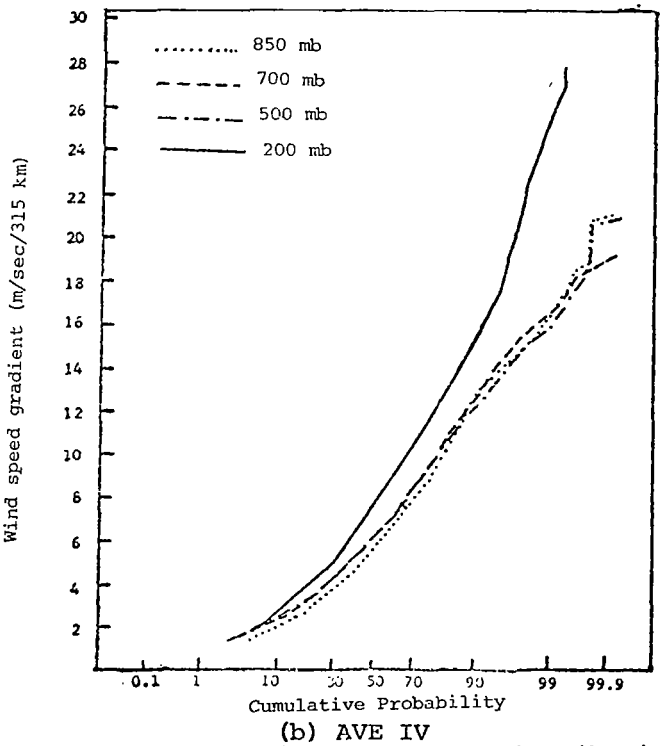

(b) AVE IV

Fig. 12. Cumulative frequency distributions of wind speed gradients.

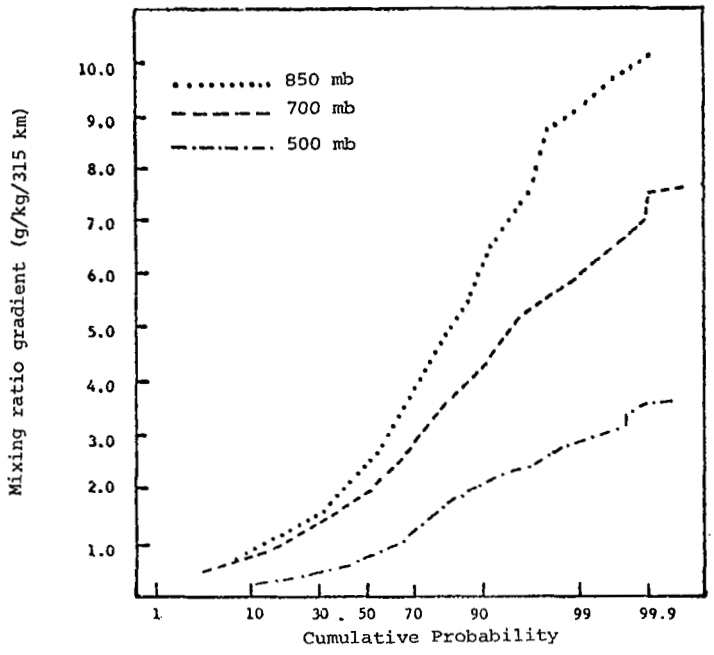

(a) AVE II

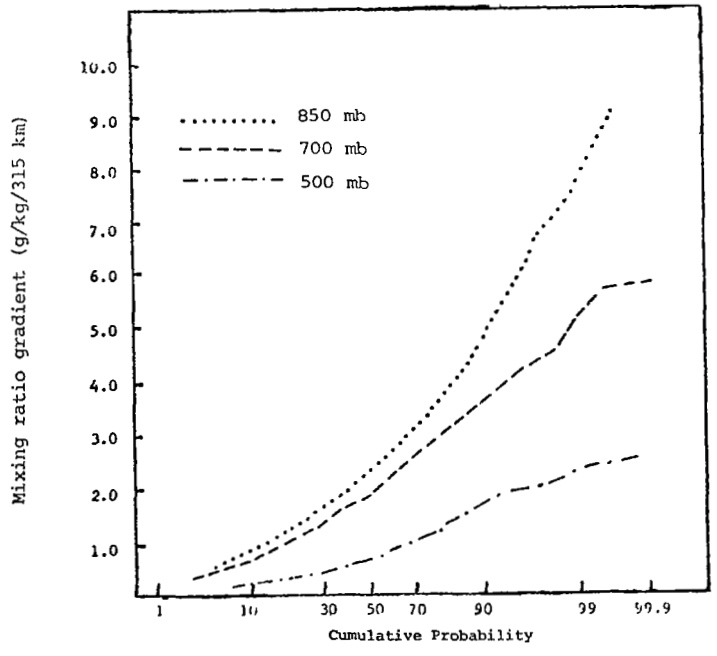

(b) AVE IV

Fig. 13. Cumulative frequency distributions of mixing ratio gradients.

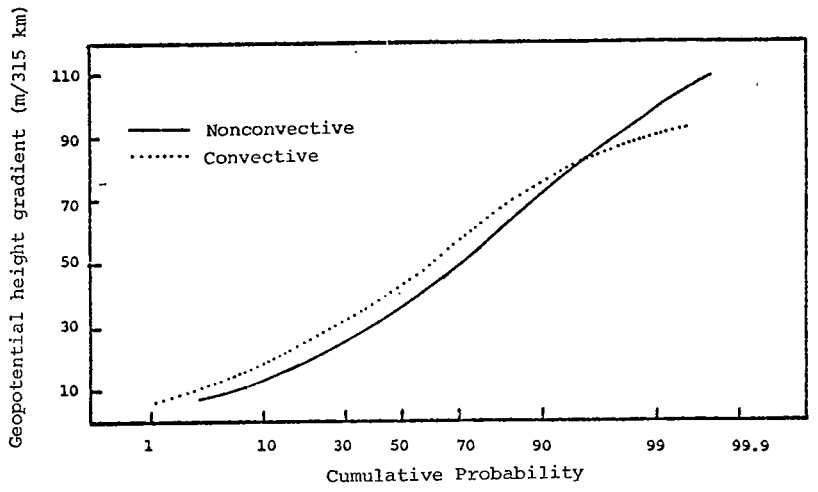

(a) 850 mb

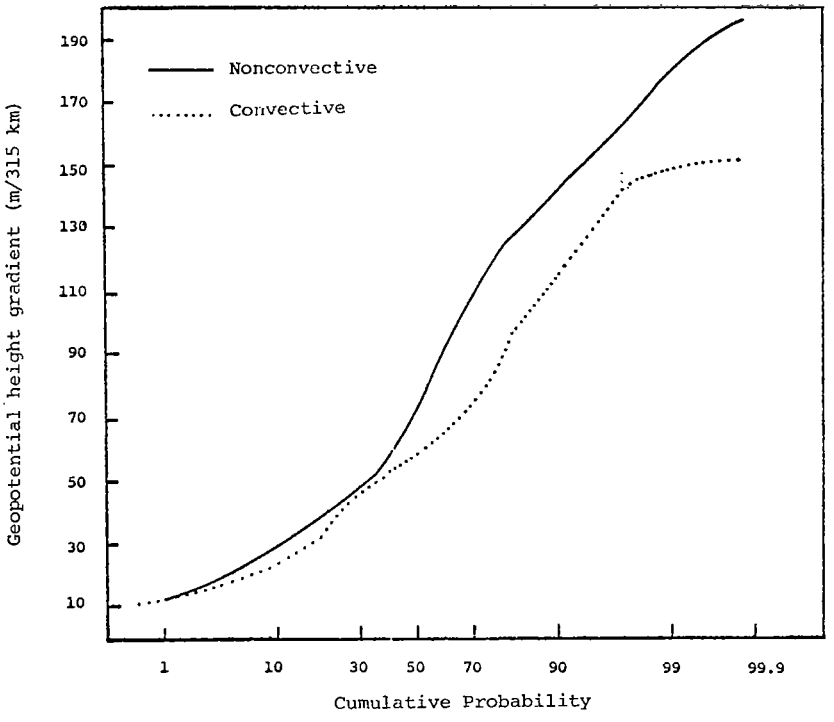

(b) 500 mb

Fig. 14. Cumulative frequency distributions of geopotential height gradients in convective and nonconvective areas of AVE II.

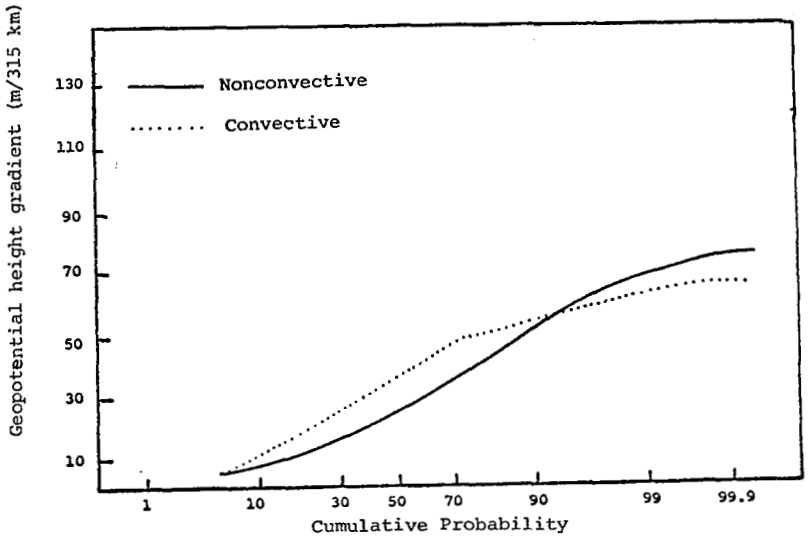

(a) 850 mb

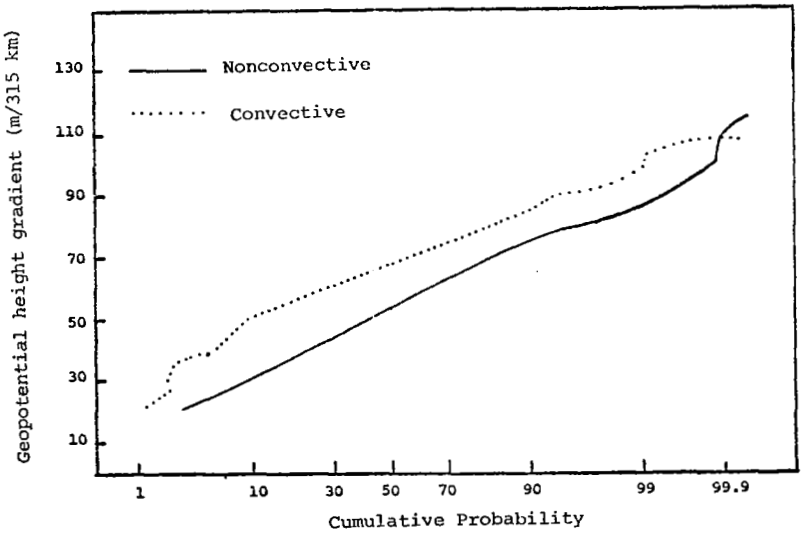

(b) 500 mb

Fig. 15. Cumulative frequency distributions of geopotential height gradients in convective and nonconvective areas of AVE IV.

while at 500 mb the gradients were larger in the nonconvective areas. In AVE IV, the results for the 850-mb level were somewhat similar to those in AVE II with approximately 95% of the gradients being larger in the convective than in nonconvective areas. But, at 500 mb in AVE IV the gradients were larger in the convective areas than in nonconvective areas.

Frequency distributions of wind speed gradients are shown for AVE II in Figs. 16a and 16b, and in Figs. 17a and 17b for AVE IV. At 850 mb, the wind speed gradients in both experiments were larger in convective than in nonconvective areas. As was the case with height gradients in AVE II, the wind speed gradients at 500 mb in AVE II were larger in the nonconvective areas. In AVE IV, the distributions at 500 mb of the gradients in nonconvective and convective areas were nearly identical.

c. Comparison of convective and nonconvective areas

As has been mentioned previously, the differences in synoptic situations between AVE II and AVE IV are considerable. Therefore, it might be expected that there would be differences when comparing the two experiments as to whether gradients are larger in the convective or nonconvective areas. A comparison of Tables 1 and 2, which were presented previously and contain information about gradients over a distance of 315 km in convective and nonconvective areas, reveals that there are many instances when this is true. For example, in AVE II mean height gradients at 500 mb were larger in the convective than in the nonconvective areas, but in AVE IV the reverse was true.

Mean geopotential height gradients at all levels in the convective areas of AVE IV were significantly larger than the mean gradients over nonconvective areas. In AVE II, the mean height gradients at 850 mb were larger in the convective than in the nonconvective areas, at 700 mb the gradients were nearly equal, and at 500 and 200 mb the mean gradients were larger in the nonconvective areas. Such results are not surprising since it is a well-known fact that precipitation often occurs in or near frontal zones;

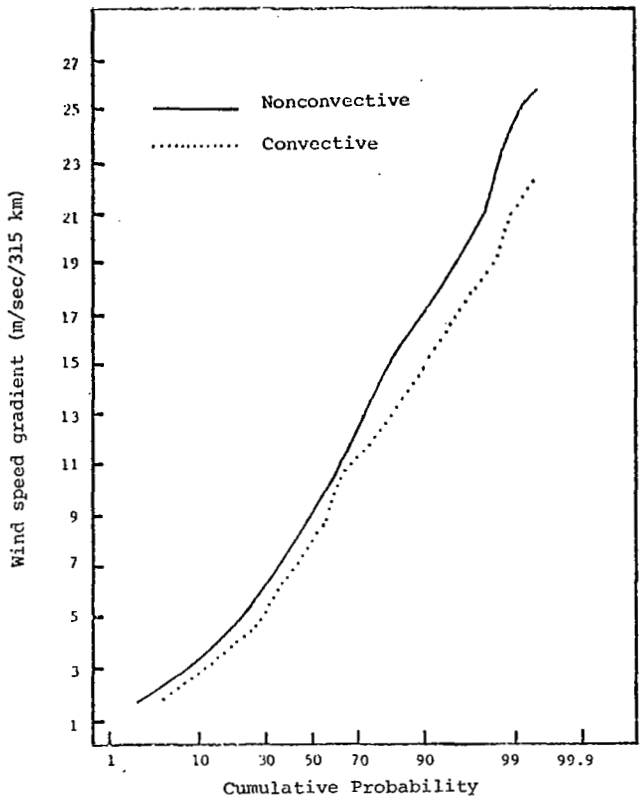

(a) 850 mb

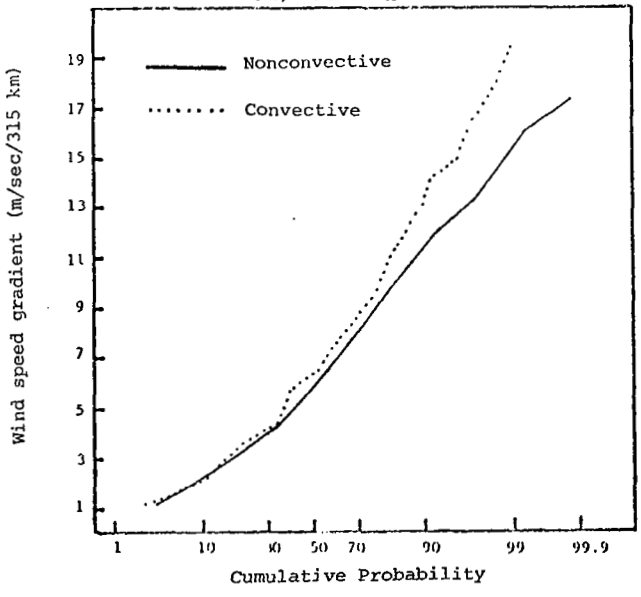

(b) 500 mb

Fig. 16. Cumulative frequency distributions of wind speed gradients in convective and nonconvective areas of AVE II.

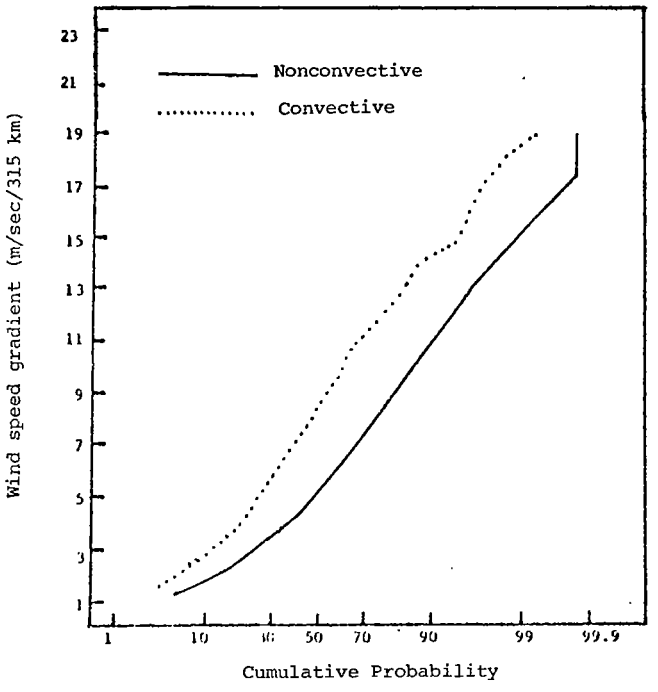

(a) 850 mb

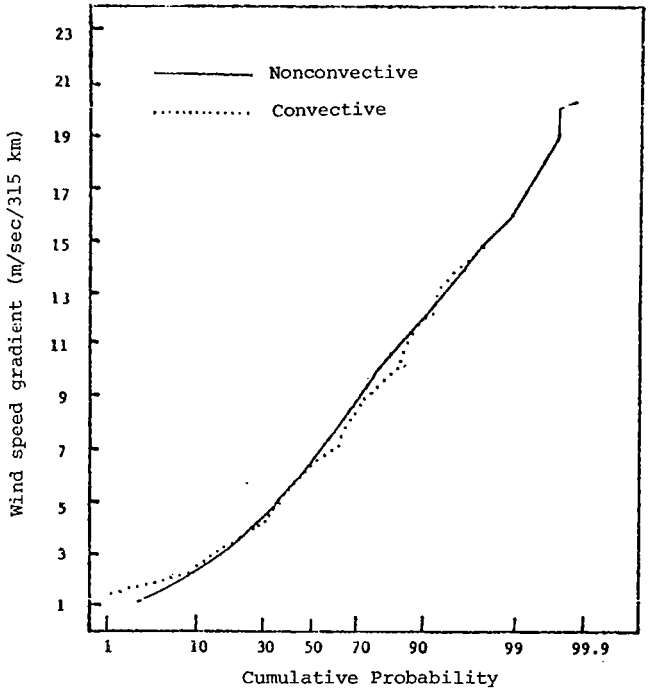

(b) 500 mb

Fig. 17. Cumulative frequency distributions of wind speed gradients in convective and nonconvective areas of AVE IV.

thus the height gradients are larger in convective areas than in nonconvective areas in the lower regions of the atmosphere. In the upper levels of AVE II, a deep trough moved through the area, whereas in AVE IV no such trough was present. It seems likely that the gradients associated with this trough tended to make the mean gradients larger in the nonconvective areas rather than in the convective areas ahead of the trough. Another interesting aspect of the height gradients was the fact that the coefficients of variation were smaller in the convective than in nonconvective areas of both experiments. This indicates that the average variability of gradients in the convective areas was smaller than elsewhere.

Mean temperature gradients at all levels in AVE IV were virtually identical in convective and nonconvective areas, but in AVE II larger gradients occurred in the nonconvective areas than in convective regions. Large temperature gradients in AVE II existed in the major trough while relatively weak gradients occurred over the convective regions ahead of the trough. An examination of the coefficients of variation reveals that the variability of temperature gradients in convective and nonconvective areas were roughly the same.

Wind speed gradients at 850 mb in both experiments were strong in the convective areas. Such a finding is consistent with findings by Miller (1967) and others who stress the importance of a low-level jet in the formation and maintenance of severe storms. While some convective activity in both experiments did occur away from the low-level jets, there was a tendency for storms to occur near the jets, which is where wind speed gradients were likely to be large. Large wind speed gradients at other levels in AVE IV did not seem to occur preferentially in either convective or nonconvective areas. In AVE II, the mean gradients at 500 and 200 mb were larger outside of the convective areas. The large wind speeds associated with the major trough appears to have been the reason for this finding.

Mixing ratio gradients in both experiments and at almost all levels were large near convective regions. Such a result is not surprising since higher levels of moisture are generally present in

the convective areas. In previous work involving AVE II, Wilson and Scoggins (1976) have shown that thunderstorm activity generally occurred in areas where the average relative humidity from surface to 500 mb was greater than 60%. Naturally, gradients across such an area with a high moisture content are likely to be larger, though this would affect gradients in the surrounding nonconvective areas, also. The coefficients of variation reveal that the variability of the mixing ratio gradients in convective areas was less extreme than that in the nonconvective areas.

Though overall statistical approaches as applied in the previous sections are likely to yield information about the average conditions in convective areas, another approach must be attempted in order to determine the differences between the gradients under the same synoptic conditions in particular storm areas and nearby nonconvective areas.

In AVE IV, means of the gradients of each of the four meteorological variables were computed for each time separately. These means for the overall, convective, and nonconvective areas of each level are given in Table 6. It should be noted that during the first four time periods (through 1500 GMT on April 24) a squall line completed most of its life cycle. The data for the convective areas during these time periods represent means obtained solely from this squall line, since convection was not present elsewhere on the grid. This squall line reached its maximum development at 0600 GMT on 24 April. The means of the gradients obtained at 1800 and 2100 GMT on 24 April and 0000 GMT on 25 April were from both decaying and developing convective systems. During the period 0600 GMT-1200 GMT, 25 April, convective activity was again confined to a single squall line, with maximum development occurring at 0600 GMT.

As can be seen in Table 6, overall height gradients at 850 and 750 mb were generally decreasing during the course of the AVE IV experiment, but gradients at 500 and 200 mb showed no consistent trends. The height gradients over the first squall line increased at all levels below 200 mb during the squall line's life cycle (data from convective areas in Table 6 for the first four time periods).

Table 6. Comparison of mean gradients in convective and nonconvective areas in AVE IV for each time period.

The numbers in parentheses beside mean 850 mb geopotential height gradients represent the number of grid points over which each mean was computed for each time period. Overall, there were 99 grid points per time period.

Time	850 mb			700 mb			500 mb			200 mb		
	Con.	Noncon.	Overall	Con.	Noncon.	Overall	Con.	Noncon.	Overall	Con.	Noncon.	Overall
24-25 April	Geopotential Height Gradients (m/315 km)											
00 GMT	30.4 (17)	39.1 (82)	37.6	43.8	42.5	42.8	67.6	55.5	57.6	131.9	97.4	103.3
06 GMT	39.6 (27)	32.2 (72)	34.2	46.6	39.3	41.3	68.0	55.6	59.0	105.9	96.3	98.9
12 GMT	37.3 (13)	30.0 (86)	30.9	47.2	37.1	38.5	69.5	52.7	54.9	92.9	85.1	86.1
15 GMT	45.7 (8)	28.5 (91)	29.9	64.0	37.5	39.6	79.1	54.8	56.8	97.6	92.9	93.3
18 GMT	34.3 (10)	27.6 (89)	28.3	47.8	37.9	38.9	58.5	56.8	57.0	79.2	95.6	94.0
21 GMT	31.7 (22)	23.0 (77)	24.9	41.0	34.5	35.9	60.4	55.3	56.4	92.4	98.0	96.8
00 GMT	26.0 (27)	23.4 (72)	24.1	39.7	33.0	34.9	69.6	53.0	57.5	108.5	94.8	98.6
06 GMT	37.1 (22)	16.3 (77)	20.9	48.3	28.5	32.9	73.6	51.0	56.1	95.6	101.6	100.3
12 GMT	37.7 (21)	18.2 (78)	22.3	51.3	28.0	32.9	66.0	49.5	53.0	90.4	92.2	91.8
24-25 April	Temperature Gradients (°C/315 km)											
00 GMT	5.2	3.2	3.5	2.6	2.6	2.6	2.7	1.9	2.0	1.2	1.5	1.5
06 GMT	3.3	3.3	3.3	2.0	2.6	2.4	2.8	1.9	2.2	2.8	1.8	2.1
12 GMT	2.7	3.4	3.3	2.0	2.5	2.4	1.8	2.1	2.1	2.9	1.8	2.0
15 GMT	2.7	3.4	3.3	2.4	2.4	2.4	1.1	2.3	2.2	2.4	1.8	1.9
18 GMT	3.0	3.0	3.0	2.6	2.4	2.4	2.0	2.1	2.1	1.8	1.9	1.9
21 GMT	2.9	3.1	3.1	2.4	2.9	2.8	1.8	2.2	2.1	2.2	1.8	1.9
00 GMT	3.7	3.0	3.2	3.3	2.5	2.7	2.7	2.2	2.3	1.9	2.1	2.0
06 GMT	3.3	3.6	3.6	2.9	3.0	3.0	2.2	2.4	2.4	1.8	2.7	2.5
12 GMT	3.3	3.8	3.7	3.2	3.0	3.0	1.6	2.5	2.3	2.7	2.6	2.6

Table 6. (continued)

Time	850 mb			700 mb			500 mb			200 mb		
	Con.	Noncon.	Overall	Con.	Noncon.	Overall	Con.	Noncon.	Overall	Con.	Noncon.	Overall
24-25 April	Wind Speed Gradients (m/sec/315 km)											
00 GMT	7.7	5.4	5.8	5.2	6.0	5.9	3.7	4.8	4.6	5.5	6.2	6.1
06 GMT	10.5	6.0	7.2	7.3	5.7	6.2	6.7	5.5	5.8	10.9	6.9	8.0
12 GMT	12.3	6.5	7.3	6.5	7.5	7.4	6.6	7.1	7.0	7.1	8.6	8.4
15 GMT	13.3	7.2	7.7	8.2	8.6	8.6	5.1	8.3	8.0	8.5	7.5	7.6
18 GMT	9.8	5.6	6.1	8.0	7.8	7.8	7.8	7.3	7.3	8.0	7.3	7.3
21 GMT	6.0	5.8	5.8	6.7	7.8	7.6	7.4	6.7	6.8	6.3	8.0	7.6
00 GMT	6.8	5.2	5.6	5.1	5.7	5.5	5.0	5.8	5.6	8.7	8.8	8.8
06 GMT	8.6	4.8	5.6	5.2	5.3	5.3	9.1	8.6	8.7	11.2	11.2	11.2
12 GMT	6.1	5.7	5.8	8.3	6.1	6.5	8.4	7.4	7.6	13.1	9.4	10.2
24-25 April	Mixing Ratio Gradients (g/kg/315 km)											
00 GMT	3.5	2.5	2.6	1.9	2.2	2.1	.6	1.0	.9			
06 GMT	3.4	2.7	2.9	2.3	1.7	1.9	.9	.8	.8			
12 GMT	3.7	2.6	2.7	2.4	2.0	2.0	.9	1.0	1.0			
15 GMT	2.2	2.9	2.8	2.1	2.0	2.0	1.4	.8	.9			
18 GMT	1.6	2.3	2.3	1.8	1.5	1.6	.7	.7	.7			
21 GMT	1.8	2.3	2.2	2.2	2.1	2.1	.7	.8	.7			
00 GMT	3.6	2.9	3.1	2.6	2.3	2.4	.7	.8	.8			
06 GMT	2.2	2.7	2.6	2.1	1.7	1.8	1.4	.6	.8			
12 GMT	1.9	2.4	2.3	3.1	2.0	2.3	1.2	.6	.7			

Gradients over the second squall line increased at 850 and 700 mb and decreased at 500 and 200 mb during the portion of the life cycle of this system that could be studied (data from the convective area for the last two time periods).

Overall temperature gradients at the 850- and 700-mb levels either remained constant or decreased slightly until 1800 GMT, and then tended to increase during the remaining time periods (Table 6). Overall temperature gradients at 500 and 200 mb tended to remain constant, then increased slightly by the end of the experiment. Gradients computed over the first squall line during its life cycle tended to decrease at most levels (convective areas in Table 6, 0000 GMT-1500 GMT, 24 April). Temperature gradients computed over the second squall line did not show consistent trends from one pressure level to another (convective areas in Table 6, 0600 GMT-1200 GMT, 25 April).

The overall wind speed gradients in Table 6 increased at all levels except 200 mb until 1800 GMT, 24 April, and generally decreased thereafter. At 200 mb, the trend was not consistent. Over the first squall line, these gradients at 850 mb tended to increase during the life cycle of the system. Inconsistent results were obtained for other pressure levels in the first squall line, and for the second squall line when comparing the trends at different pressure levels.

Overall mixing ratio gradients in Table 6 showed no consistent trends. During the life cycle of the first squall line, mixing ratio gradients increased at 500 mb, but showed no consistent trends at other pressure levels. Again, inconsistent results were obtained for the second squall line when comparing trends at different pressure levels.

Since different areas of the grid were experiencing very different synoptic situations in AVE II, two regions were designated, and gradients in the convective and nonconvective areas within each region were studied. In the midwest region, a warm front moved northeastward through the region's center, while a cold front advanced rapidly southeastward. The other region considered was in

the southeast. Fronts did not affect this region much, but a Gulf cyclone moved to the region's center by the end of the time periods studied. Only 850- and 500-mb levels were considered in this study, and the time periods ran consecutively from 1200 GMT on 11 May 1974 through 0300 GMT on 12 May 1974. Mean gradients in the convective and nonconvective areas of each region were computed for each time period, and prestorm and poststorm gradients, as previously defined, were considered. Figure 18 shows the boundaries of the midwest and southeast regions.

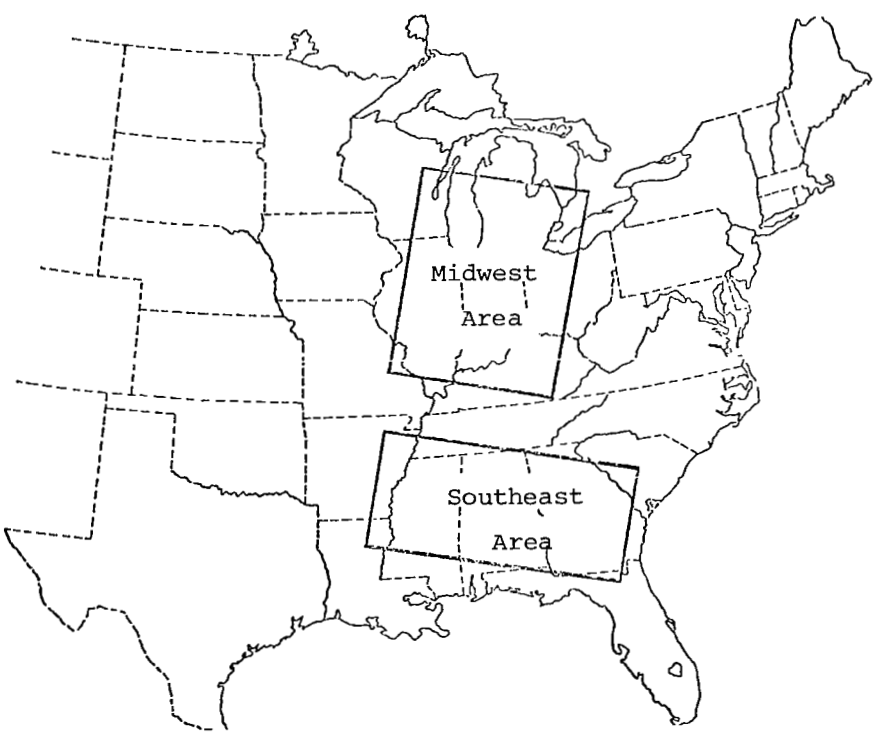

Fig. 18. Boundaries of midwest and southeast areas used in AVE II.

Table 7 shows the means of the gradients in convective and nonconvective areas for each separate time in both the southeast and midwest regions. Unfortunately in both the southeast and midwest regions, nearly the entire areas were covered by convection at times, while at other times only a few data points were affected by storms. Comparisons between convective and nonconvective areas become rather difficult because of the unequal number of grid points within each area, but to have used a larger area would not have allowed obtaining gradients for uniform synoptic situations within each area. In most cases, maximum gradients in both the convective and nonconvective areas occurred at the same time maximum gradients occurred over each region.

Mean height gradients at 850 mb were larger in the convective than in nonconvective areas in the southeast region and until 1800 GMT in the midwest region. At 500 mb, the mean height gradients were larger during most of the time periods in convective areas in the southeast region, and were larger in storm areas than in nonstorm areas for the first half of the time periods studied in the midwest. The influence of the approaching trough was seen at 500 mb in the midwest region as a general increase in the magnitude of the gradients. No consistent trend was established for the southeast region.

The influence of the trough in the midwest region was also seen in overall temperature gradients, which increased steadily at 500 mb during the time periods studied. A general increase of the temperature gradients was noted also at 850 mb in this region. In the southeast, the overall temperature gradients at 500 mb weakened until 2100 GMT and increased afterwards, while at 850 mb the opposite was true.

Wind speed gradients at both levels in the midwest and southeast regions were stronger in the convective than in nonconvective areas. The fact that jet streams were occurring at both levels over the convective areas in both the midwest and southeast regions tended to cause large wind speed gradients in those areas. The gradients at 850 mb in the midwest region decreased during most of the time

Table 7. Comparison of mean gradients in convective and nonconvective areas in AVE II for each time period.

The numbers in parentheses beside mean 850 mb geopotential height gradients represent the number of grid points over which each mean was computed for each time period in each region. Overall, there were 18 grid points per time period in the Southeast region and 20 per time period in the Midwest region.

Time	850 mb						500 mb					
	Southeast Region			Midwest Region			Southeast Region			Midwest Region		
	Con.	Noncon.	Overall	Con.	Noncon.	Overall	Con.	Noncon.	Overall	Con.	Noncon.	Overall
11-12 May	Geopotential Height Gradients (m/315 km)											
12 GMT	42 (3)	29 (15)	31	61 (9)	37 (11)	48	42	30	32	64	48	55
15 GMT	45 (4)	39 (14)	40	65 (7)	55 (13)	58	29	35	34	80	78	79
18 GMT	47 (8)	35 (10)	41	62 (12)	50 (8)	57	32	32	32	87	76	83
21 GMT	53 (8)	42 (10)	47	51 (17)	60 (3)	52	52	43	47	89	116	93
00 GMT	47 (13)	38 (5)	44	42 (13)	61 (7)	49	43	41	43	87	140	105
03 GMT	45 (10)	40 (8)	43	30 (5)	50 (15)	45	41	31	46	114	117	116
11-12 May	Temperature Gradients (°C/315 km)											
12 GMT	1.2	0.7	0.8	3.4	3.0	3.1	4.0	2.1	2.4	1.1	1.1	1.1
15 GMT	1.2	1.1	1.1	3.3	3.3	3.3	4.0	1.9	2.3	1.2	1.5	1.4
18 GMT	1.6	1.5	1.5	3.1	3.4	3.2	1.4	1.4	1.4	2.3	2.1	2.2
21 GMT	2.7	2.6	2.6	3.7	3.2	3.6	1.3	1.5	1.4	2.7	4.0	2.9
00 GMT	2.1	2.5	2.2	4.6	4.7	4.7	1.5	2.0	1.6	3.0	5.1	3.7
03 GMT	1.6	1.4	1.5	4.0	4.3	4.3	1.0	2.8	1.9	6.8	5.8	6.0

Table 7 (continued)

Time	850 mb						500 mb					
	Southeast Region			Midwest Region			Southeast Region			Midwest Region		
	Con.	Noncon.	Overall	Con.	Noncon.	Overall	Con.	Noncon.	Overall	Con.	Noncon.	Overall
11-12 May	Wind Speed Gradients (m/sec/315 km)											
12 GMT	9.6	6.9	7.3	10.1	7.3	8.5	7.0	5.6	5.8	7.9	5.6	6.7
15 GMT	10.9	7.8	8.5	6.1	6.9	6.7	7.1	5.3	5.7	12.2	7.3	9.0
18 GMT	12.9	8.9	10.7	6.3	4.7	5.7	5.7	5.4	5.5	10.1	5.6	8.3
21 GMT	10.2	8.5	9.3	6.4	3.4	5.9	10.0	7.1	8.4	9.4	5.1	8.7
00 GMT	7.8	7.1	7.6	3.2	3.5	3.3	3.8	3.1	3.6	8.7	10.4	9.3
03 GMT	6.6	4.3	5.6	5.2	5.1	5.1	4.1	5.5	4.7	6.0	5.7	5.8
11-12 May	Mixing Ratio Gradients (g/kg/315 km)											
12 GMT	6.4	3.9	4.3	4.5	4.8	4.7	0.5	1.0	0.9	0.9	0.9	0.9
15 GMT	3.4	2.7	2.8	4.3	3.5	3.8	1.4	0.8	0.9	1.1	1.4	1.3
18 GMT	3.6	4.5	4.1	3.6	4.4	3.9	0.8	1.3	1.1	1.5	1.1	1.3
21 GMT	2.1	2.7	2.4	4.1	4.0	4.1	1.7	1.5	1.6	1.8	1.1	1.7
00 GMT	1.9	2.1	1.9	3.5	4.3	3.8	1.8	2.4	1.9	1.8	2.2	1.9
03 GMT	1.4	1.7	1.4	3.2	2.3	2.6	0.9	1.9	1.3	1.8	1.3	1.4

periods studied, while those in the southeast increased until 1800 GMT, and decreased thereafter. No consistent trends were noticeable in either region at 500 mb.

Mixing ratio gradients at 500 mb tended to increase in both regions during the time periods studied. At 850 mb, the gradients generally decreased in both regions. Large mixing ratio gradients did not seem to occur preferentially in either convective or nonconvective areas in either region.

Results from the study of prestorm and poststorm gradients in the midwest and southeast regions of AVE II are given in Table 8. Height gradients at both 850 and 500 mb tended to be smaller after the storms than before in the southeast, but an increase in the magnitude of the height gradients at both levels was noted in the midwest. Temperature gradients at both levels generally increased as the storms moved through the midwest, but there was only a weak tendency for this to occur in the southeast region. At 850 mb, maximum gradients in wind speed occurred before or during the storms in both the southeast and midwest regions, and decreased as storms moved out of an area. At 500 mb, the reverse was true with maximum gradients following the storms in both areas, though the observed differences were small. Mixing ratio gradients decreased slightly following the storms in both regions at 850 mb, and increased after, or during, the storms at 500 mb.

The results from this study of the midwest region indicate that the general synoptic situation is perhaps dominating any changes brought about by convection, or else the convection is acting in such a way as to reinforce the synoptic gradient fields. The changes in the gradients in the southeast region were most likely to indicate changes brought about by the convection, since the southeast region was not dominated by as strong a synoptic-scale system as was evident in the midwest.

A prestorm and poststorm study of gradients in AVE IV was performed involving all pressure levels and all nine times. In addition, a comparison of gradients involved when the intensity of the convective areas differed from one time to the next was made using the

Table 8. Means of gradients in AVE II over areas in which the status of convection changed.

Numbers in parentheses indicate number of grid points studied in each region and at each level.

		Prestorm to Storm			Storm to Poststorm		
Geopotential Height			(m/315 km)			(m/315 km)	
850 mb	Southeast Region	40	(17)	44	34	(10)	38
	Midwest Region	55	(18)	56	58	(22)	59
500 mb	Southeast Region	38	(17)	43	33	(10)	30
	Midwest Region	81	(18)	90	96	(22)	113
Temperature			(°C/315 km)			(°C/315 km)	
850 mb	Southeast Region	1.6		2.2	1.7		2.1
	Midwest Region	3.7		3.7	4.9		4.8
500 mb	Southeast Region	1.9		1.7	2.3		2.0
	Midwest Region	2.2		2.9	2.7		3.9
Wind Speed			(m/sec/315 km)			(m/sec/315 km)	
850 mb	Southeast Region	8.2		8.4	10.5		6.5
	Midwest Region	6.8		6.2	5.1		4.5
500 mb	Southeast Region	5.6		5.0	5.8		7.0
	Midwest Region	7.0		8.0	7.2		8.2
Mixing Ratio			(g/kg/315 km)			(g/kg/315 km)	
850 mb	Southeast Region	3.0		2.9	2.7		2.9
	Midwest Region	3.8		3.6	3.8		3.4
500 mb	Southeast Region	1.0		1.3	1.3		1.7
	Midwest Region	1.2		1.7	1.5		1.5

MDR values. The MDR code and rates of precipitation associated with particular MDR values have been discussed previously. Since there were no strong synoptic weather systems in AVE IV, the effects of the convective areas upon the gradients was easier to determine than was the case in AVE II. Results from this study are contained in Table 9.

In areas where there was only moderate convective activity or less (MDR $\leq$ 3) before or after the storms, the height gradients at 850 and 700 mb were generally strongest in the prestorm areas, and tended to decrease in the subsequent storm and poststorm areas. At 500 and 200 mb, the height gradients tended to reach their maximum in the storm areas one time period prior to the storm's subsequent dissipation, or movement out of the area. In contrast to this pattern, in areas where there was strong convective activity ($4 \leq$ MDR ≤ 7) present before or after intense storms (MDR ≥ 8), gradients at all levels tended to be largest during the most severe storms, or in the areas of strong activity following the intense storms.

Temperature gradients in regions where there was moderate activity or less before or after the storms, tended to increase at 850 mb as the storms developed, and reached a maximum in the storm areas prior to subsequent dissipation. Relatively small changes were noted at other levels as the status of convective activity changed. In areas where there was strong activity present before or after intense storms, the maximum gradients occurred before or during the intense storms except at 200 mb where the largest gradients occurred following the severe storms.

Wind speed gradients tended to be largest over the poststorm areas. Particularly strong gradients were noted over areas of strong convective activity following severe storms. Mixing ratio gradients followed much the same pattern as the wind speed gradients, though the differences were relatively small.

A comparison of the values in Table 8 for the southeast area and the corresponding values of MDR $\leq$ 3 and MDR $\geq$ 4 in Table 9 reveals a broad similarity in the changes in gradients observed

Table 9. Means of gradients in AVE IV over areas in which the status of convection changed.

Numbers in parentheses beside 850 mb geopotential height gradients indicate number of grid points studied.

Prestorm - Storm Means of Gradients								
	MDR=0,1 to MDR≥2			MDR=0,1 to MDR≥4			MDR≤3 to MDR≥4			4≤MDR≤7 to MDR≥8		
Geopotential Height	(m/315 km)			(m/315 km)			(m/315 km)			(m/315 km)		
850 mb	31.6	(110)	30.2	35.6	(44)	32.2	36.7	(86)	33.9	27.2	(10)	27.5
700 mb	40.0		39.6	43.4		43.1	44.1		44.0	40.5		43.1
500 mb	58.4		59.2	65.3		64.7	64.8		66.0	65.4		67.0
200 mb	98.5		94.7	105.7		101.1	101.4		98.9	103.7		106.3
Temperature	(°C/315 km)			(°C/315 km)			(°C/315 km)			(°C/315 km)		
850 mb	3.0		3.1	2.7		3.0	2.9		3.1	3.5		3.9
700 mb	2.7		2.8	3.0		2.9	2.9		2.8	3.2		3.0
500 mb	2.1		2.0	2.3		2.0	2.1		2.1	2.3		2.7
200 mb	1.9		2.3	1.9		2.3	1.9		2.2	1.7		2.2
Wind Speed	(m/sec/315 km)			(m/sec/315 km)			(m/sec/315 km)			(m/sec/315 km)		
850 mb	6.0		6.3	5.8		7.0	5.9		7.3	9.6		8.3
700 mb	6.4		7.1	6.5		6.7	6.2		6.1	7.1		5.8
500 mb	6.9		7.4	7.1		7.8	6.5		7.0	5.5		7.6
200 mb	7.0		9.6	6.1		9.2	6.2		9.3	6.7		8.8
Mixing Ratio	(g/kg/315 km)			(g/kg/315 km)			(g/kg/315 km)			(g/kg/315 km)		
850 mb	2.7		2.6	2.8		2.7	2.6		2.6	2.9		2.6
700 mb	2.1		2.1	2.4		2.3	2.3		2.3	1.3		2.4
500 mb	.7		.8	.8		.9	.8		.9	.5		.8

Table 9 (continued)

Storm - Poststorm Means of Gradients												
	MDR≥2 to MDR=0,1			MDR≥4 to MDR=0,1			MDR≥4 to MDR≤3			MDR≥8 to 4≤MDR≤7		
Geopotential Height	(m/315 km)			(m/315 km)			(m/315 km)			(m/315 km)		
850 mb	31.1	(123)	28.2	25.7	(40)	21.0	30.7	(92)	24.5	40.9	(13)	38.5
700 mb	39.9		37.4	41.1		34.8	43.6		36.9	46.4		51.7
500 mb	60.3		58.0	66.6		57.2	68.0		60.9	70.5		76.7
200 mb	102.0		97.2	114.3		105.1	112.0		107.1	88.3		107.7
Temperature	(°C/315 km)			(°C/315 km)			(°C/315 km)			(°C/315 km)		
850 mb	3.4		3.2	4.2		3.7	3.9		3.6	2.6		3.0
700 mb	2.7		2.9	2.9		2.8	2.6		2.7	2.8		2.8
500 mb	2.4		2.3	2.7		2.5	2.6		2.7	2.0		2.2
200 mb	2.0		2.1	2.3		2.4	2.3		2.3	2.4		2.8
Wind Speed	(m/sec/315 km)			(m/sec/315 km)			(m/sec/315 km)			(m/sec/315 km)		
850 mb	7.1		6.1	7.8		6.0	8.3		6.7	9.4		11.5
700 mb	7.6		7.1	6.4		6.1	6.4		7.7	5.9		8.8
500 mb	7.7		7.3	7.4		7.1	7.1		8.0	4.7		10.2
200 mb	8.9		7.5	9.8		8.0	9.9		9.4	4.8		9.8
Mixing Ratio	(g/kg/315 km)			(g/kg/315 km)			(g/kg/315 km)			(g/kg/315 km)		
850 mb	2.9		2.7	3.3		3.2	3.2		2.8	3.3		2.9
700 mb	2.4		2.1	2.4		2.4	2.3		2.5	2.5		2.7
500 mb	1.0		.8	.9		.8	1.0		.9	.9		1.4

as convection moved through the southeast region of AVE II and the entire area of AVE IV. Since the convection in both cases was in the form of squall lines, these changes may be regarded as typical of such regions. Height gradients at 850 mb were largest in the prestorm or storm areas immediately after the storm formation, and at 500 mb the largest gradients were within the storm areas. Temperature and wind speed gradients at both levels were larger in the storm or poststorm areas than in the prestorm areas. The largest mixing ratio gradients also tended to occur over the storm or poststorm areas in AVE IV and at 500 mb in AVE II. These results agree for the most part with the conclusions of Ninomiya (1971b) concerning gradients near convective areas.

Time continuity of analyzed gradient fields of geopotential height, temperature, wind speed, and mixing ratio were also used to give some idea of the structure of the mesoscale systems. Only the gradient fields at 850 and 500 mb for one time each in AVE II and AVE IV are shown. These observation times were chosen to illustrate significant events occurring during each of the experiments. In AVE II at 2100 GMT, 11 May, the convection was more widespread than at any of the other times. In AVE IV, this was so at 0600 GMT, 24 April, and was the time a squall line was at its maximum strength. Composite MDR charts are shown in Figs. 19 and 20 for the times at which the analyzed fields are shown for AVE II and AVE IV, respectively. Convective areas, as defined by the MDR charts, are shown by stippling on the analyzed maps of gradient fields.

Analyzed fields of the geopotential height gradient are shown in Fig. 21. In AVE IV and in most areas of AVE II, the largest gradients at 850 mb occurred ahead of or in the convective areas. The small area of gradients greater than 60 m/315 km in southern Georgia in AVE II was positioned ahead of a squall line. A squall line also was present west of the area of large height gradients in eastern Michigan and over Lake Huron. At 500 mb in AVE IV, and in the southeast area of AVE II, large gradients were located over the convective areas. In both cases, these gradients were larger than

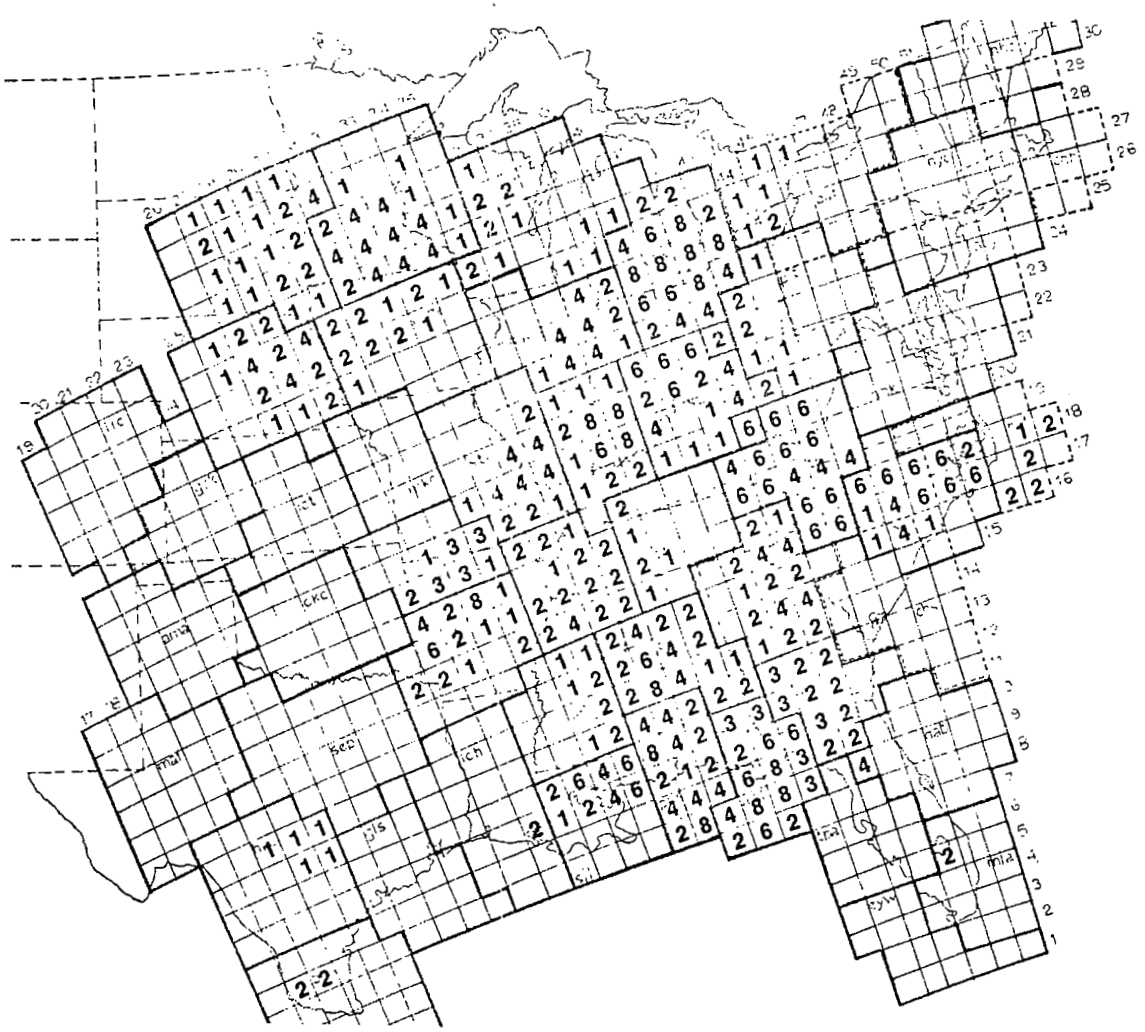

Fig. 19. Composite digital radar (MDR) chart for 2100 GMT, 11 May 1974.

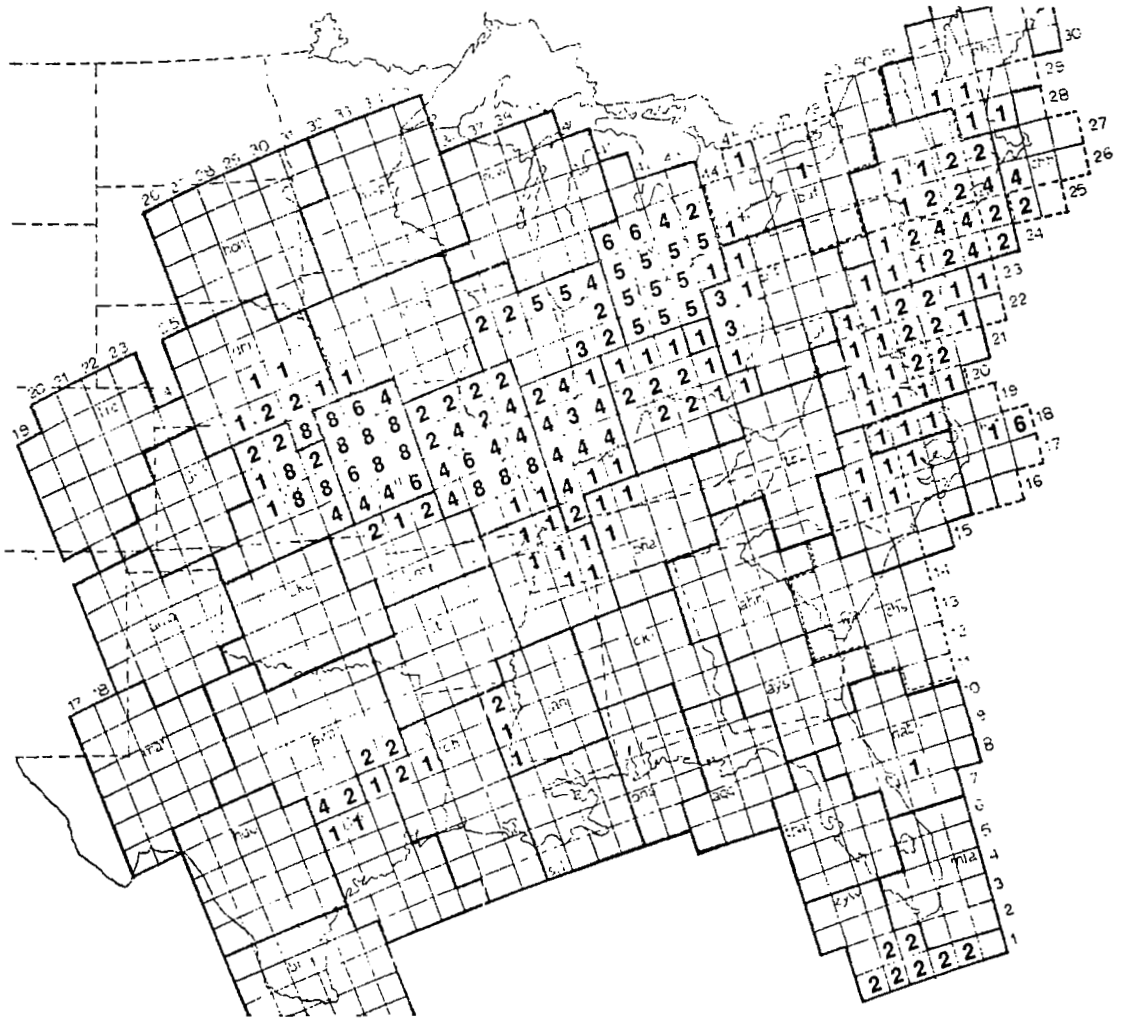

Fig. 20. Composite digital radar (MDR) chart for 0600 GMT, 24 April, 1975.

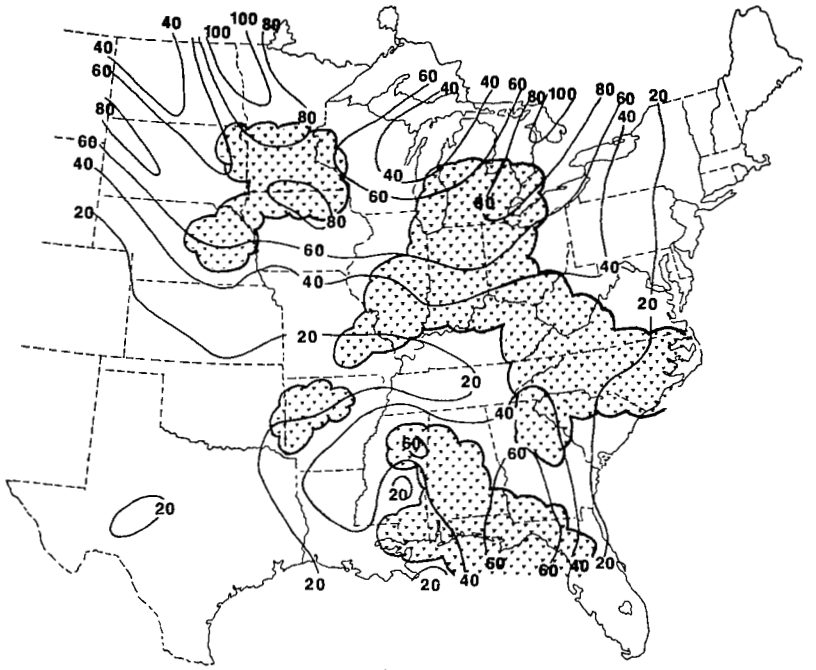

(a) 850 mb, 2100 GMT, 11 May 1974

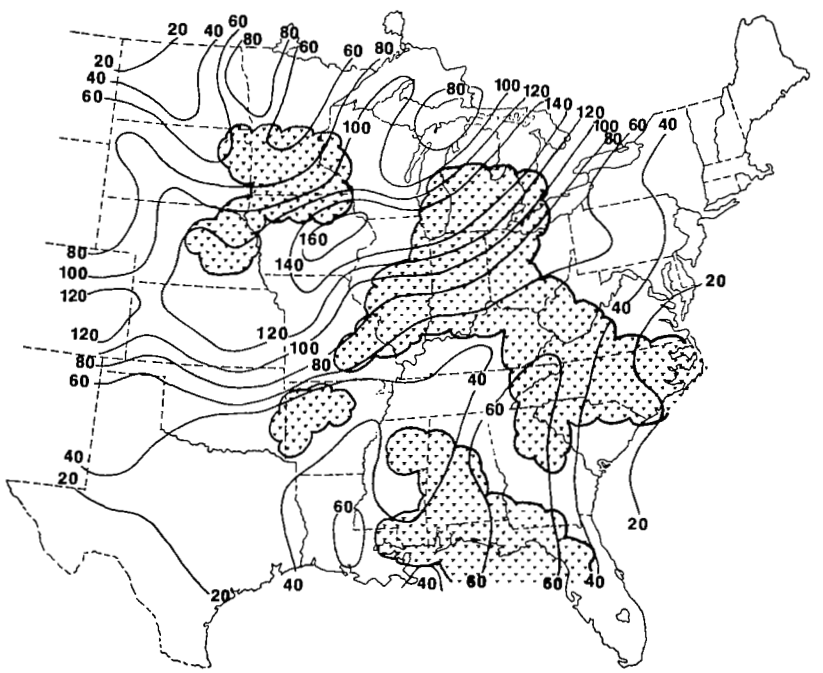

(b) 500 mb, 2100 GMT, 11 May 1974

Fig. 21. Geopotential height gradient fields (m/315 km).

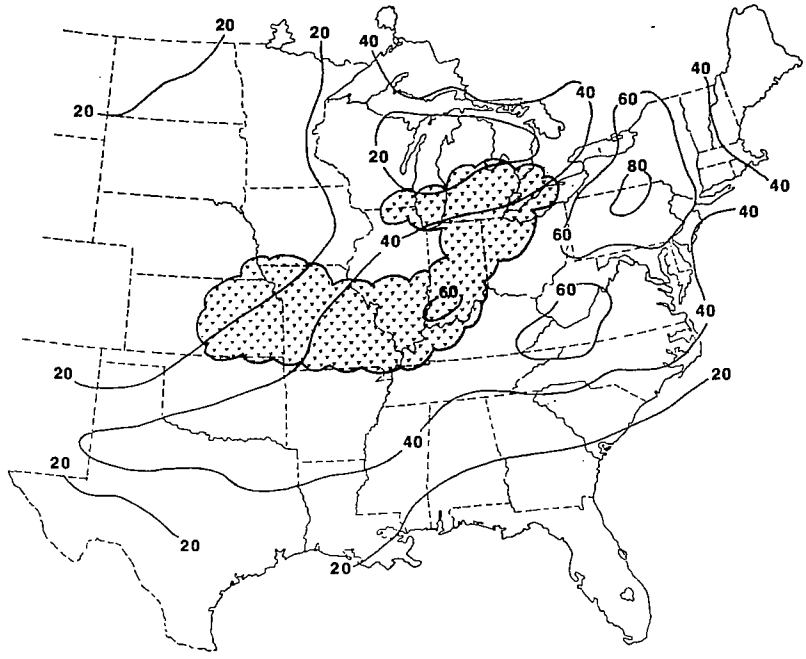

(c) 850 mb, 0600 GMT, 24 April 1975

(d) 500 mb, 0600 GMT, 24 April 1975

Fig. 21. (Continued)

60 m/315 km. The influence of the strong trough at this level is readily seen in the midwest region of AVE II, where an area of gradients greater than 160 m/315 km is located between the two convective areas. The convective area over Minnesota and Nebraska in AVE II was due to an intense short wave moving through the major trough at this time.

Figure 22 shows analyzed fields of temperature gradients. In both AVE experiments, the largest temperature gradients in or near convective areas at 850 mb occurred generally over the storm or poststorm areas, and from the analyzed temperature fields (not shown), it was obvious that a thermal ridge existed through the convective areas of both experiments, particularly in AVE IV. At 500 mb, the thermal gradient in AVE IV was largest to the northwest of the storm area, but in AVE II, the largest gradients were in response to the cold air associated with the short wave in the Nebraska region. An area of large temperature gradients in AVE II also existed to the northwest of the squall line in Michigan, but no large gradients were associated with the squall line in the southeast.

Analyzed fields of wind speed gradients are presented in Fig. 23. The largest gradients in wind speed at 850 mb occurred in the convective areas in AVE IV. At this time, areas containing localized wind speeds near 25 m sec^{-1} occurred over West Virginia and eastern Oklahoma. Convection was occurring northwest of these areas, and it was in the convective area where wind speed gradients were the largest. In AVE II, maximum wind speed gradients occurred over the convection in the southeast, east of the squall line in Michigan, and near the trough in the Nebraska area. At 500 mb in AVE IV, a jet with speeds of 30 m sec^{-1} was occurring within the convective area. At this particular time, the maximum wind speed gradients were ahead of the convective area, with a secondary region of large gradients behind the storms. In AVE II, the maximum wind speed gradients at 500 mb were occurring with the jet associated with the trough in the north central states, and a secondary region of large gradients occurred over the convective area in the south central states.

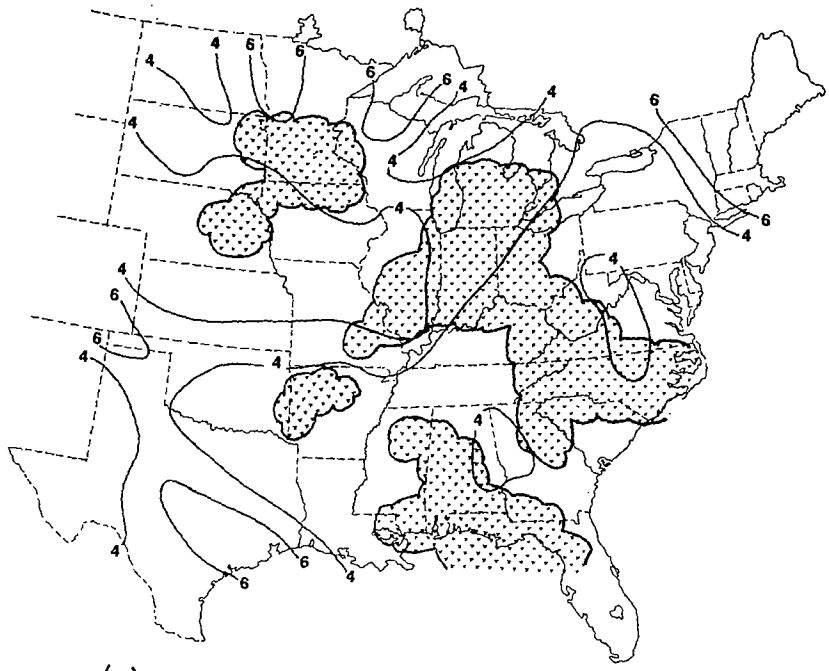

(a) 850 mb, 2100 GMT, 11 May 1974

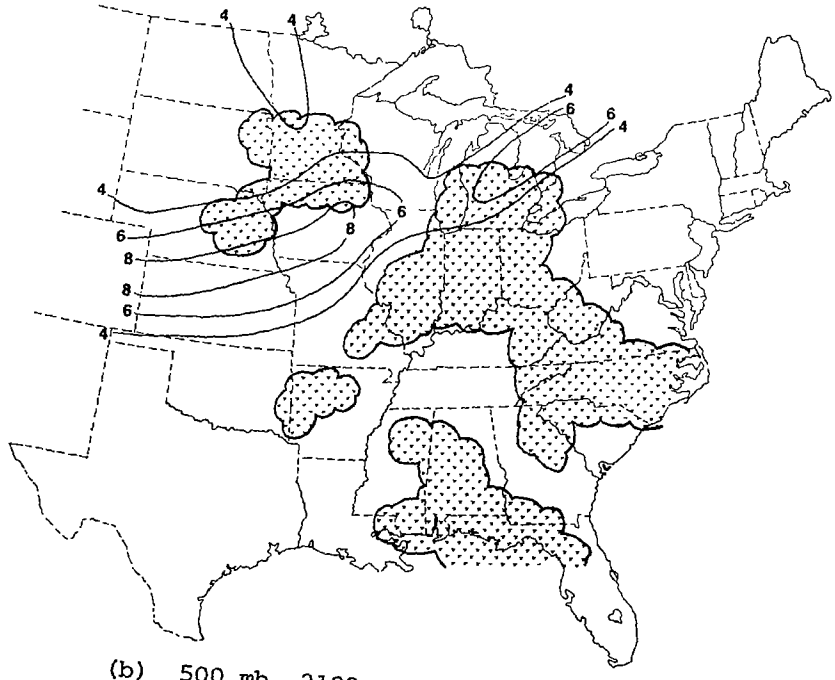

(b) 500 mb, 2100 GMT, 11 May 1974

Fig. 22. Temperature gradient fields (°C/315 km).

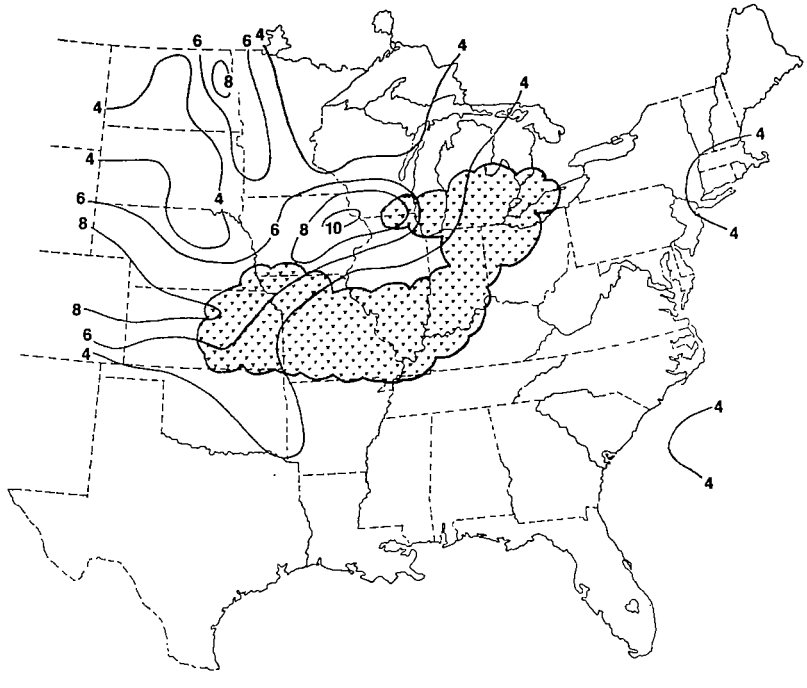

(c) 850 mb, 0600 GMT, 24 April 1975

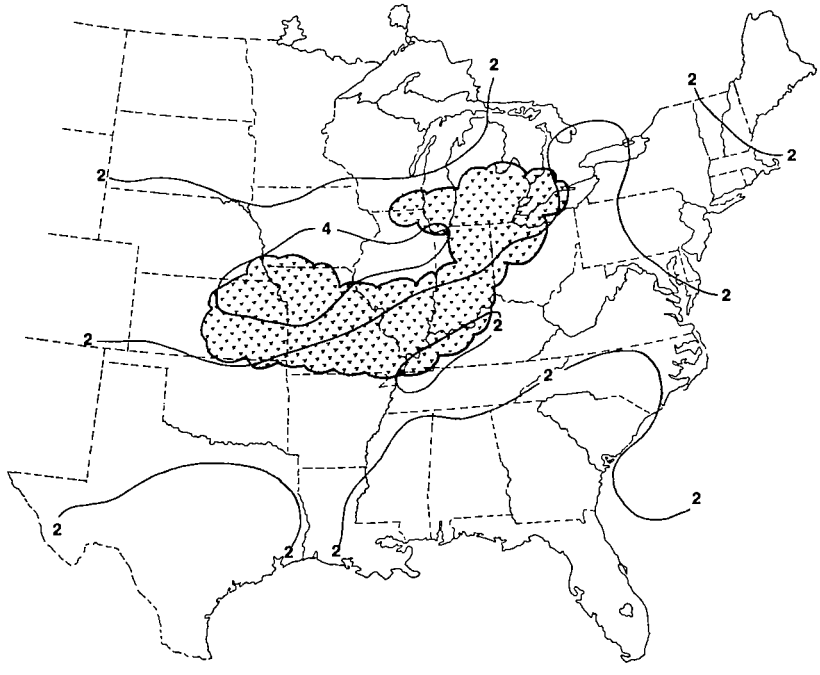

(d) 500 mb, 0600 GMT, 24 April 1975

Fig. 22. (Continued)

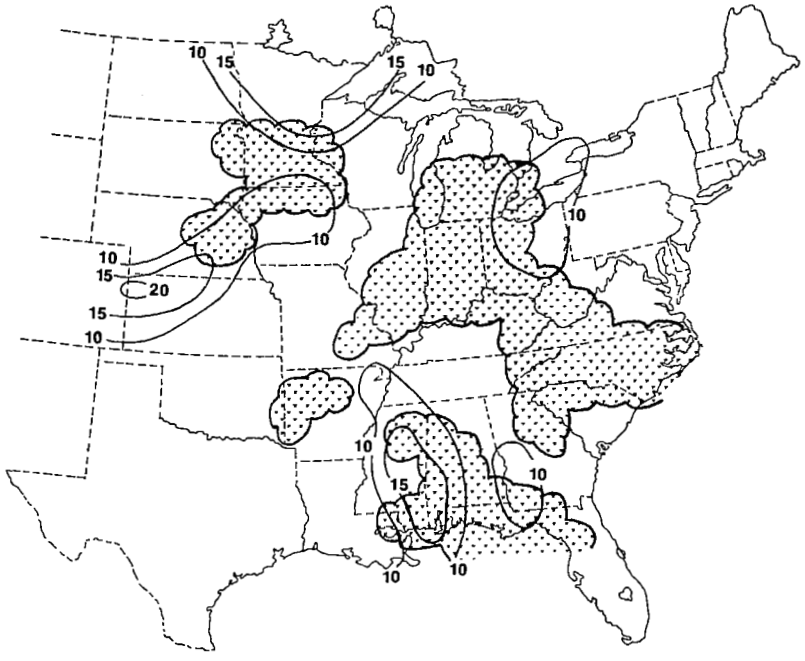

(a) 850 mb, 2100 GMT, 11 May 1974

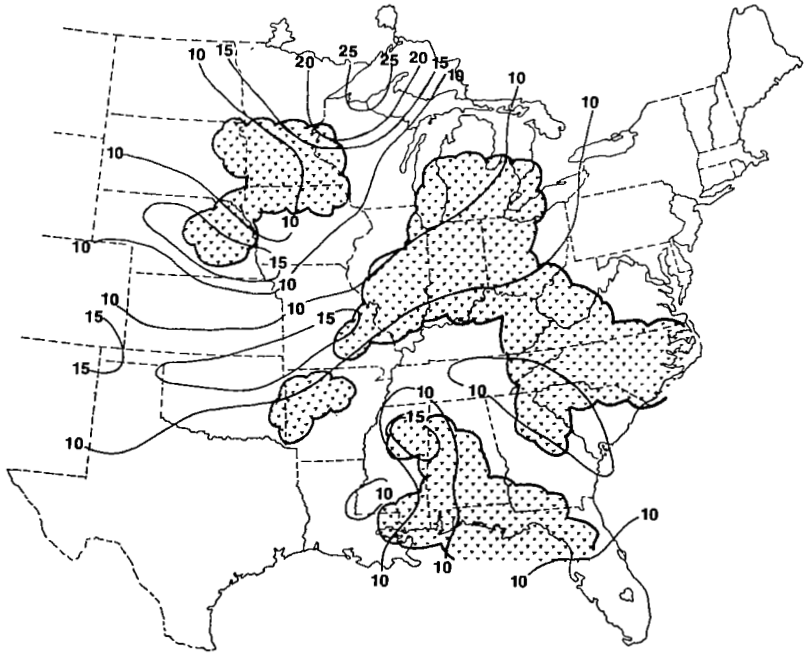

(b) 500 mb, 2100 GMT, 11 May 1974

Fig. 23. Wind speed gradient fields (m/sec/315 km).

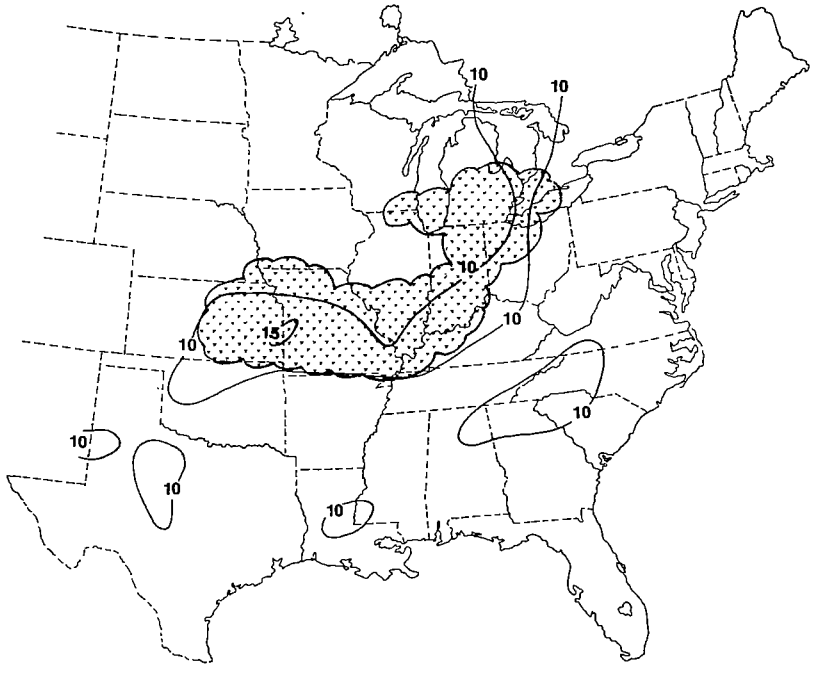

(c) 850 mb, 0600 GMT, 24 April 1975

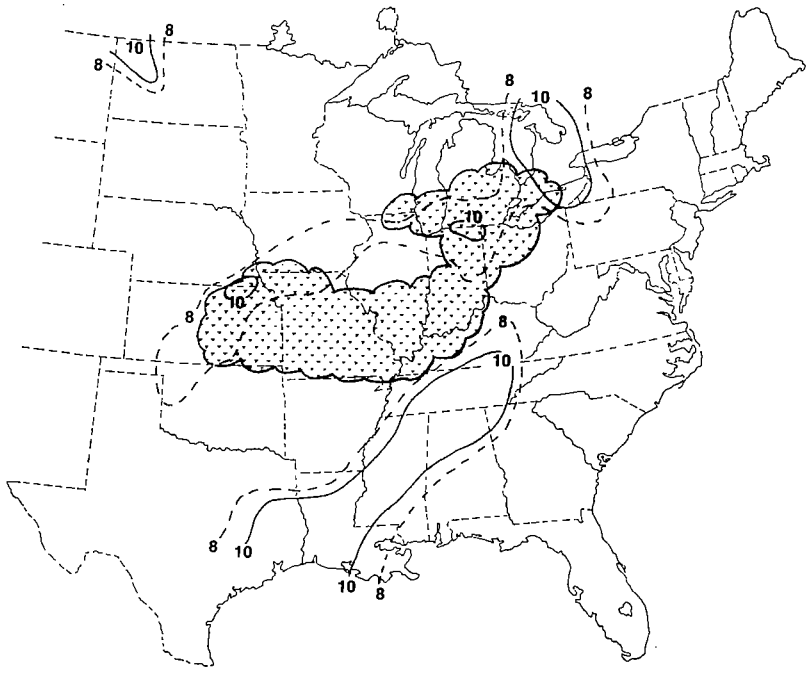

(d) 500 mb, 0600 GMT, 24 April 1975

Fig. 23. (Continued)

Figure 24 shows fields of mixing ratio gradients for both experiments. At 850 mb in AVE IV, mixing ratio gradients larger than 7 gm/kg/315 km occurred along a dry line in the Texas panhandle northeastward into the convective region. In AVE II, the largest gradients at 850 mb occurred in a band from Lake Michigan southwestward into Texas, which is just west of the main storm area. At 500 mb in both experiments, the largest gradients occurred generally in the convective areas.

Overall, the pattern of gradients in the convective areas is suggestive of a front, even when there is no front near the convective area, as was the case in the southeast area of AVE II. Petterson (1956) mentioned the fact that squall lines act as fronts, but noted that squall lines tend to move through the same air mass instead of between air masses, as real fronts do. The fact that strong moisture gradients occur to the rear of storms has been noted by Miller (1967). In AVE IV, definite changes, particularly in the thermal field, could be attributed to the convective areas, but in AVE II these changes were largely masked by the overall synoptic situation.

d. Gradients versus MDR values

A comparison of gradient values versus MDR data was made using the AVE IV data; the results are shown in Table 10. Four categories of MDR values were considered, and the value of the gradient at each grid point was assigned to one or more of these categories. Means and standard deviations were computed for the data contained in each division. The four MDR categories correspond to areas with little or no convection, areas with no convection through moderate intensity, areas with convection of strong through intense activity, and finally areas of intense convective activity.

Height gradients at all levels tended to increase in value with the intensity of precipitation, although there was a decrease in the mean gradient value from the "strong through intense" category to the "intense" category. This decrease in the magnitude of height gradients for the intense category was most marked at the 850-mb level,

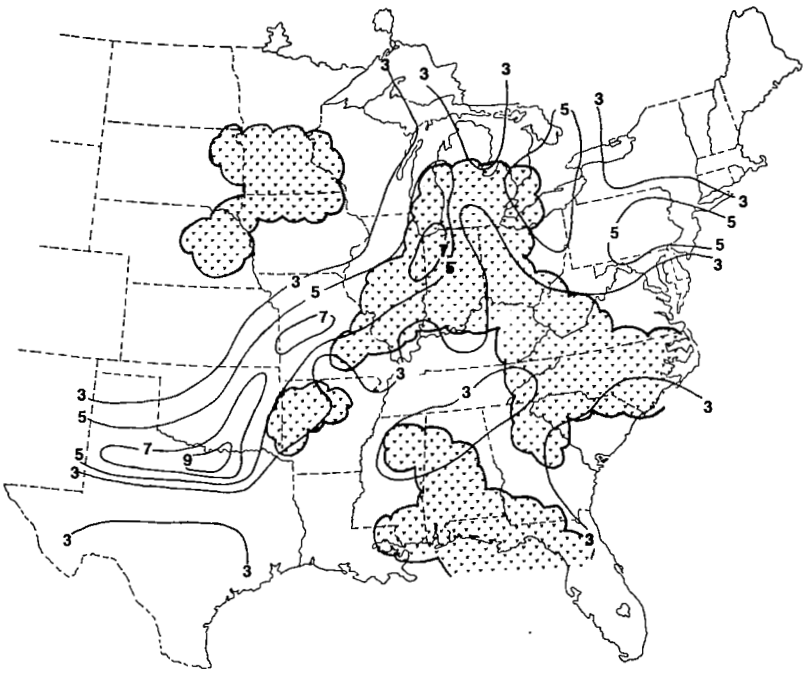

(a) 850 mb, 2100 GMT, 11 May 1974

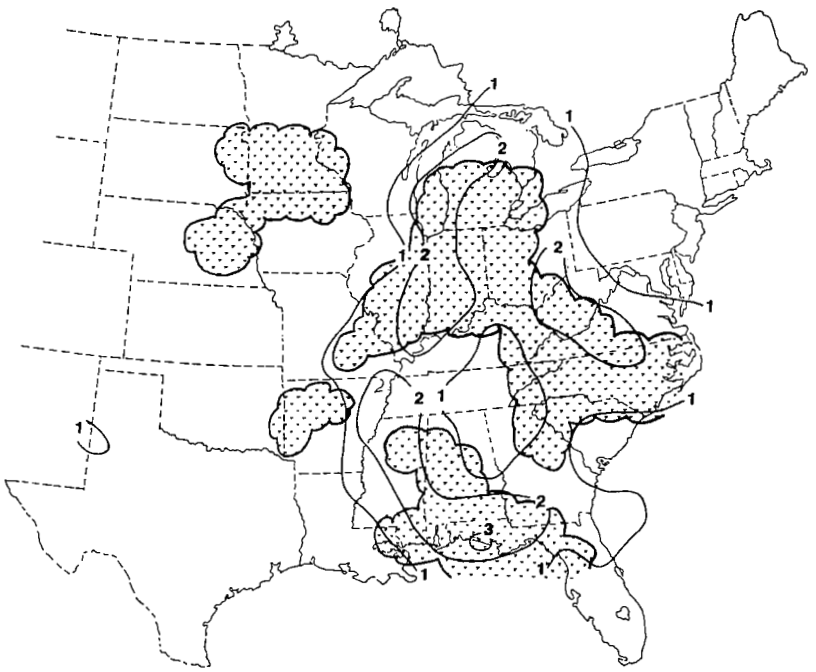

(b) 500 mb, 2100 GMT, 11 May 1974

Fig. 24. Mixing ratio gradient fields (g/kg/315 km).

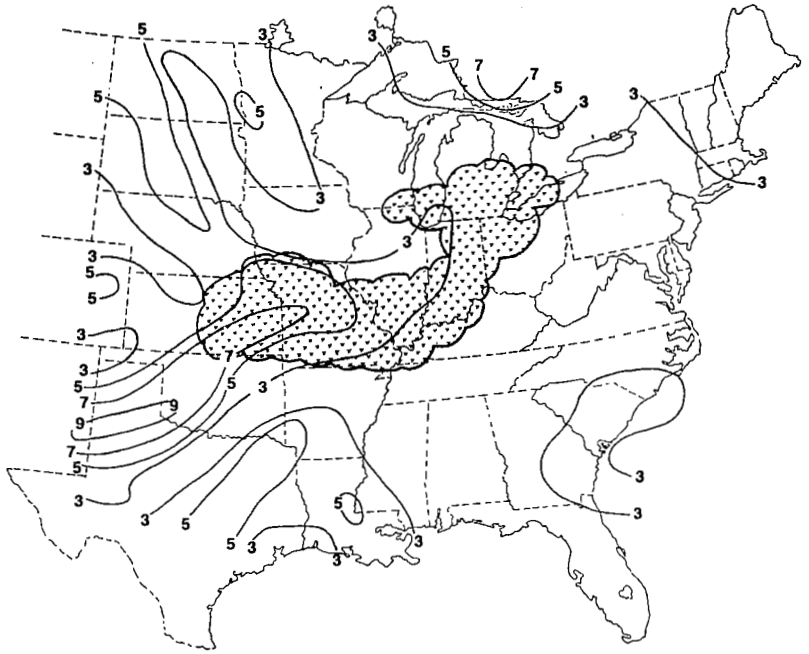

(c) 850 mb, 0600 GMT, 24 April 1975

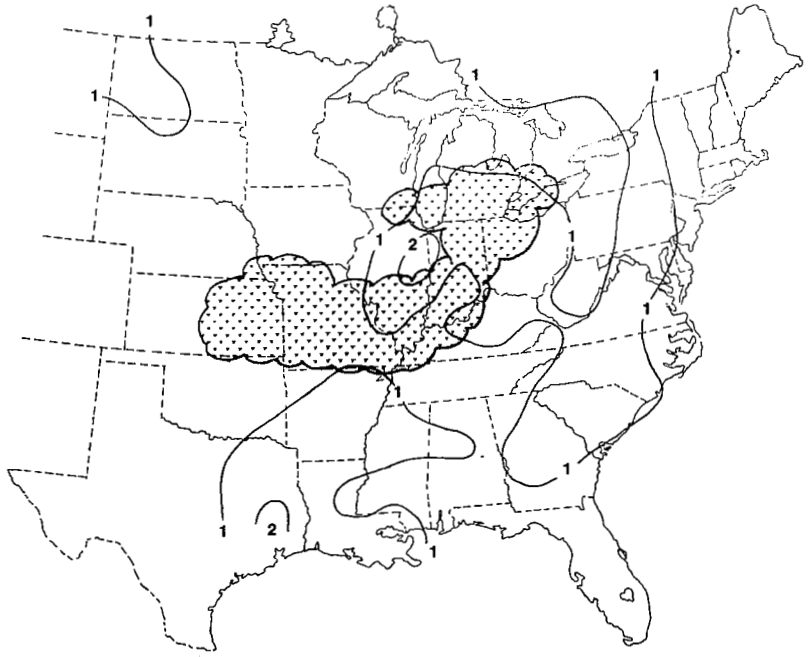

(d) 500 mb, 0600 GMT, 24 April 1975

Fig. 24. (Continued)

Table 10. Comparison of gradient values versus MDR data for AVE IV.

	MDR=0,1 - 475 grid points		MDR=0,1,2,3 - 724 grid points		4≤ MDR≤ 9 - 167 grid points		MDR=8,9 - 61 grid points	
	Mean	Standard Deviation	Mean	Standard Deviation	Mean	Standard Deviation	Mean	Standard Deviation
Geopotential Height	(m/315 km)		(m/315 km)		(m/315 km)		(m/315 km)	
850 mb	23.7	15.5	26.6	16.7	34.7	15.8	28.5	14.5
700 mb	32.8	13.3	35.5	15.0	46.2	15.0	40.3	11.8
500 mb	51.1	16.5	53.9	16.6	67.8	14.4	65.8	11.3
200 mb	94.5	28.3	94.7	28.4	100.9	30.7	105.3	22.6
Temperature	(°C/315 km)		(°C/315 km)		(°C/315 km)		(°C/315 km)	
850 mb	3.4	2.0	3.0	1.9	3.4	1.9	3.8	2.1
700 mb	2.7	1.2	2.7	1.2	2.7	1.1	3.0	1.1
500 mb	2.2	1.1	2.2	1.1	2.2	1.2	2.5	1.1
200 mb	1.9	1.2	2.0	1.2	2.2	1.2	2.0	1.1
Wind Speed	(m/sec/315 km)		(m/sec/315 km)		(m/sec/315 km)		(m/sec/315 km)	
850 mb	5.5	3.3	5.8	3.5	8.5	4.3	8.3	3.9
700 mb	6.2	3.6	6.8	3.9	6.5	3.4	6.3	3.0
500 mb	6.6	3.6	6.9	3.8	6.7	3.6	6.3	3.5
200 mb	7.4	4.5	8.2	5.1	9.1	5.6	7.8	4.9
Mixing Ratio	(g/kg/315 km)		(g/kg/315 km)		(g/kg/315 km)		(g/kg/315 km)	
850 mb	2.7	1.6	2.6	1.6	2.8	1.8	3.5	1.9
700 mb	1.8	1.1	1.9	1.1	2.3	1.2	2.3	1.1
500 mb	0.7	0.5	0.8	0.6	0.9	0.6	0.9	0.6

and was not as noticeable in the upper levels. Temperature gradients were virtually the same for all categories, but increased slightly for the intense category. An examination of the MDR data in conjunction with the analyzed fields of the meteorological variables revealed the reasons for these temperature and height variations. The MDR values of 8 or 9 occurred only when the squall lines were at their peak strength, and at such times the squall lines were near the frontal boundary. Since temperature gradients were largest here, and height gradients in the lower levels tended to be larger somewhat ahead of the front, the results for the intense category were biased in favor of larger temperature gradients and smaller height gradients, especially in the lower levels.

Wind speed gradients usually increased as the intensity of storms increased at 850 mb, but no relationship was found between the intensity of storms and wind speed gradients in the upper levels. Mixing ratio gradients were largest in the "strong to intense" and "intense" categories at all levels.

These results are consistent with what has been stated in previous sections concerning gradients in and near convective areas. The convective storms in AVE IV tended to form near baroclinic regions and reached their peak strength soon after formation. As the squall line moved away from the front, the storms and gradient patterns weakened, but still acted in the lower levels in such a way as to resemble a front.

e. Comparison of gradients in AVE II and AVE IV

The frequency distributions of gradients in AVE II and AVE IV have been shown to be similar in form, though not in magnitude. The mean magnitude of gradients at all levels in AVE II was larger than that of AVE IV, indicating a more sharply defined synoptic situation in AVE II than in AVE IV. The variability of gradients was also larger in AVE II than in AVE IV. Whereas a cold pocket embedded in a short wave at 500 mb, and other well-defined mesosystems with strong gradients existed in AVE II, the gradients associated with mesosystems in AVE IV were not as strong as those in AVE II.

These differences had an impact upon the type of precipitation present, and upon what could be learned from the precipitation areas concerning gradients. The gradients associated with the general synoptic situation in most of the AVE II grid tended to overshadow differences in the gradients which resulted from convection. The squall lines in AVE IV, and the squall line in the southeast in AVE II were similar and produced noticeable changes in the gradient fields. These changes in the thermal, wind speed, and moisture fields were similar to those found by Ninomiya (1971a) in a similar situation, though the changes found by Ninomiya were more pronounced.

7. SUMMARY AND CONCLUSIONS

a. Summary

An objective analysis of the gradients of four atmospheric variables has been carried out using Manually Digitized Radar data and rawinsonde data from AVE II and AVE IV. The gradient fields of geopotential height, temperature, wind speed, and mixing ratio were produced using data that are unique in temporal spacing. Cumulative frequency distributions of the gradients were determined for 850, 700, 500, and 200 mb in convective and nonconvective areas, and statistical methods were applied to determine changes in the gradient patterns brought about by convective activity.

b. Conclusions

The following conclusions were reached for the AVE II and AVE IV experiments:

1) Gradients in general
   a) As gradients are determined over longer distances, the magnitude and variability of the gradients decrease.
   b) Large variability in the gradient patterns occurs over periods of 3 h. Much of the variability may possibly be related to subsynoptic disturbances.
   c) Cumulative frequency distributions of the gradients for AVE II and AVE IV were similar in shape, but not necessarily in magnitude. Since the synoptic situations in the two cases were so different, it may be inferred that frequency distributions of gradients over large areas will be generally similar in shape.
2) Comparison of gradients in convective and nonconvective areas
   a) Distributions of the gradients over convective and nonconvective areas are also similar in shape, but not necessarily in magnitude. Positive skewness of the distributions generally exists, and the standard deviation of a particular gradient distribution is roughly one-half the size of the mean.

b) The largest mixing ratio gradients occur near convective areas. At 850 mb, larger geopotential height and wind speed gradients are found in convective than in nonconvective areas. No general relationship between convective and nonconvective areas holds for the gradients at other levels or for other parameters. Height and mixing ratio gradients, relative to their mean values, are somewhat less variable in convective than in nonconvective areas.

3) Gradients relative to storm areas

a) Convection, at least on a small scale, may occur without appearing to disturb the gradient patterns. No particular gradient pattern of any of the atmospheric variables, or combinations of them, necessarily implies convection.

b) Squall lines appear to be a special case of convection where there appear to be typical gradient patterns and trends. The most intense storms form near fronts or other baroclinic disturbances where gradient values tend to be large. Though height gradients at 850 mb are larger in the prestorm areas or in areas immediately after the storms have formed, at other levels, the height gradients are larger over the storm areas or poststorm areas. Gradients of temperature, wind speed, and mixing ratio also are larger over the storm or poststorm areas. The storm interacts with the environment so as to maintain these gradients.

REFERENCES

Barnes, S. L., 1964: A technique for maximizing detail in numerical weather map analysis. J. Appl. Meteor., 3, 396-409.

Barr, S., W. K. Widger, Jr., I. A. Miller, and R. Stanton, 1971: Objective subsynoptic upper level analysis. J. Appl. Meteor., 10, 410-417.

Boucher, R. J., 1973: Mesoscale history of a small patch of clear air turbulence. J. Appl. Meteor., 12, 814-821.

Fankhauser, J. C., 1969: Convective processes resolved by a mesoscale rawinsonde network. J. Appl. Meteor., 8, 778-798.

_____, 1974: The derivation of consistent fields of wind and geopotential height from mesoscale rawinsonde data. J. Appl. Meteor., 13, 637-646.

Foster, D. S. and R. M. Reap, 1975: Thunderstorms and severe local storm frequency distributions for 1974 derived from Manually Digitized Radar data and severe local storms reports. Preprints 9th Conf. Severe Local Storms, Norman, Amer. Meteor. Soc., 64-67.

Fucik, N. F. and R. E. Turner, 1975: Data for NASA's AVE IV experiment: 25-mb sounding data and synoptic charts, NASA Technical Memorandum TM X-64952.

Fuelberg, H. E., 1974: Reduction and error analysis of the AVE II pilot experiment data, NASA Contractor Report CR-120496.

_____, and R. E. Turner, 1975: Data for NASA's AVE III experiment: 25-mb sounding data and synoptic charts, NASA Technical Memorandum TM X-64938.

Harley, W. S., 1971: Convective storms diagnosis and prediction using two layer combined indices of potential and latent stability in combination with other special and standard significators. Preprints 7th Conf. Severe Local Storms, Kansas City, Amer. Meteor. Soc., 23-30.

House, D. C., 1960: Remarks on the optimum spacing of upper-air observations. Mon. Wea. Rev., 88, 97-100.

Kreitzberg, C. W., 1968: The mesoscale wind field in an occlusion. J. Appl. Meteor., 7, 53-67.

Lewis, J. M., Y. Ogura, and L. Gidel, 1974: Large-scale influences upon the generation of a mesoscale disturbance. Mon. Wea. Rev., 102, 545-559.

Miller, R. C., 1967: Notes on analysis and severe-storm forecasting procedures of the military weather warning center. AWS Tech. Report 200, 170 pp.

_____, 1969: Forecasting the degree of intensity of severe thunderstorms. Preprints 6th Conf. Severe Local Storms, Chicago, Amer. Meteor. Soc., 197-201.

Ninomiya, K., 1971a: Mesoscale modification of synoptic situations from thunderstorm development as revealed by ATS III and aerological data. J. Appl. Meteor., 10, 1103-1121.

_____, 1971b: Dynamical analysis of outflow from tornado-producing thunderstorms as revealed by ATS III pictures. J. Appl. Meteor., 10, 275-294.

Ostle, B. and R. W. Mensing, 1975: Statistics in Research, Ames, Iowa, The Iowa State University Press, 596 pp.

Petterssen, S., 1956: Weather Analysis and Forecasting: Volume II, Weather and Weather Systems, New York, McGraw-Hill Book Company, Inc., 266 pp.

Reap, R. M., 1975: Thunderstorm and severe weather probabilities based on model output statistics--No. 3, Technical Procedures Bulletin No. 138, National Weather Service, Silver Springs, Md., 4 pp.

_____, and M. A. Alaka, 1969: An objective quasi-Lagrangian index for predicting convective weather outbreaks. Preprints 6th Conf. Severe Local Storms, Chicago, Amer. Meteor. Soc., 119-124.

Saucier, W. J., 1955: Principles of Meteorological Analysis, Chicago, The University of Chicago Press, 438 pp.

Scoggins, J. R., 1975: Meteorological variables vs CAT in the stratosphere: a statistical approach. J. of Aircraft, 12, 567-571.

_____, and O. E. Smith, 1973: Data for the first NASA atmospheric variability experiment (AVE I), Part I: Data tabulation, NASA Technical Memorandum TM X-2938.

_____, and R. E. Turner, 1975: 25-mb sounding data and synoptic charts for NASA's AVE II pilot experiment, NASA Technical Note TN D-7832.

_____, J. E. Wood, H. E. Fuelberg, and W. L. Read, 1972: An investigation of relationships between meso- and synoptic scale phenomena, NASA Contractor Report CR-2030.

Wilson, G. S. and J. R. Scoggins, 1976: Atmospheric structure and variability in areas of convective storms determined from 3-h rawinsonde data, NASA Contractor Report CR-2678.

APPENDIX

Rawinsonde Stations Participating in AVE II Experiment

Station Number	Location
11001 (MSF)	Marshall Space Flight Center, Alabama
22001 (OUN)	Norman, Oklahoma
22002 (FSI)	Ft. Sill, Oklahoma
22003 (LNS)	Lindsay, Oklahoma
22004 (FTC)	Ft. Cobb, Oklahoma
22005 (CHK)	Chickasha, Oklahoma
201 (EYW)	Key West Florida
202 (MIA)	Miami, Florida
208 (CHS)	Charleston, South Carolina
211 (TPA)	Tampa, Florida
213 (AYS)	Waycross, Georgia
221 (VPS)	Eglin AFB, Florida
226 (MGM)	Montgomery, Alabama
232 (BVE)	Booothville, Louisiana
235 (JAN)	Jackson, Mississippi
240 (LCH)	Lake Charles, Louisiana
248 (SHV)	Shreveport, Louisiana
250 (BRO)	Brownsville, Texas
255 (VCT)	Victoria, Texas
260 (SEP)	Stephenville, Texas
261 (DRT)	Del Rio, Texas
265 (MAF)	Midland, Texas
304 (HAT)	Hatteras, North Carolina
311 (AHN)	Athens, Georgia
317 (GSO)	Greensboro, North Carolina
327 (BNA)	Nashville, Tennessee
340 (LIT)	Little Rock, Arkansas
349 (UMN)	Monette, Missouri
363 (AMA)	Amarillo, Texas
402 (WAL)	Wallops Island, Virginia
405 (IAD)	Dulles Airport, Virginia
425 (HTS)	Huntington, West Virginia
429 (DAY)	Dayton, Ohio
433 (SLO)	Salem, Illinois
451 (DOC)	Dodge City, Kansas
456 (TOP)	Topeka, Kansas
486 (JFK)	Kennedy Airport, New York
494 (CHH)	Chatam, Massachusetts
518 (ALB)	Albany, New York
520 (PIT)	Pittsburg, Pennsylvania
528 (BUF)	Buffalo, New York
532 (PIA)	Peoria, Illinois
553 (OMA)	Omaha, Nebraska

APPENDIX (Continued)

Rawinsonde Stations Participating in AVE II Experiment

Station Number	Location
562 (LBF)	North Platte, Nebraska
606 (PWM)	Portland, Maine
637 (FNT)	Flint, Michigan
645 (GRB)	Green Bay, Wisconsin
654 (HUR)	Huron, South Dakota
655 (STC)	St. Cloud, Minnesota
662 (RAP)	Rapid City, South Dakota
712 (CAR)	Caribou, Maine
734 (SSM)	Sault Ste Marie, Michigan
747 (INL)	International Falls, Minnesota
764 (BIS)	Bismarck, North Dakota

Rawinsonde Stations Participating in AVE IV Experiment

Station Number	Location
208 (CHS)	Charleston, South Carolina
211 (TPA)	Tampa, Florida
213 (AYS)	Waycross, Georgia
220 (VPS)	Apalachicola, Florida
226 (CEN)	Centerville, Alabama
232 (BVE)	Boothville, Louisiana
235 (JAN)	Jackson, Mississippi
240 (LCH)	Lake Charles, Louisiana
248 (SHV)	Shreveport, Louisiana
255 (VCT)	Victoria, Texas
260 (SEP)	Stephenville, Texas
261 (DRT)	Del Rio, Texas
265 (MAF)	Midland, Texas
304 (HAT)	Hatteras, North Carolina
311 (AHN)	Athens, Georgia
317 (GSO)	Greensboro, North Carolina
327 (BNA)	Nashville, Tennessee
340 (LIT)	Little Rock, Arkansas
349 (UMN)	Monette, Missouri
363 (AMA)	Amarillo, Texas
402 (WAL)	Wallops Island, Virginia
405 (IAD)	Sterling, Virginia (Dulles Airport)
425 (HTS)	Huntington, West Virginia
429 (DAY)	Dayton, Ohio
433 (SLO)	Salem, Illinois

APPENDIX (Continued)

Rawinsonde Stations Participating in AVE IV Experiment

Station Number	Location
451 (DDC)	Dodge City, Kansas
456 (TOP)	Topeka, Kansas
486 (JFK)	Fort Totten, New York (Kennedy Airport)
518 (ALB)	Albany, New York
520 (PIT)	Pittsburg, Pennsylvania
528 (BUF)	Buffalo, New York
532 (PIA)	Peoria, Illinois
553 (OMA)	Omaha, Nebraska
562 (LBF)	North Platte, Nebraska
606 (PWM)	Portland, Maine
637 (FNT)	Flint, Michigan
645 (GRB)	Green Bay, Wisconsin
654 (HUR)	Huron, South Dakota
655 (STC)	St. Cloud, Minnesota
662 (RAP)	Rapid City, South Dakota
11001 (MFS)	Marshall Space Flight Center, Alabama
22002 (FSI)	Fort Sill, Oklahoma

NASA-Langley, 1977